

Simulation and Verification of Transient Events in Large Wind Power Installations

Poul Sørensen, Anca D. Hansen, Peter Christensen, Morten Mieritz, John Bech, Birgitte Bak-Jensen and Hans Nielsen

**Risø National Laboratory, Roskilde
October 2003**

Abstract Models for wind power installations excited by transient events have been developed and verified. A number of cases have been investigated, including comparisons of simulations of a three-phase short circuit, validation with measurements of tripping of single wind turbine, islanding of a group of two wind turbines, and voltage steps caused by tripping of wind turbines and by manual transformer tap-changing. A Benchmark model is also presented, enabling the reader to test own simulation results against results obtained with models developed in EMTDC and DIgSILENT.

ISBN 87-550-3030-0
ISBN 87-550-3031-9 (Internet)
ISSN 0106-2840

Print: Pitney Bowes Management Services Danmark A/S, 2003

Contents

1 Introduction 6

2 Simulation tools 9

- 2.1 Features of EMTDC and DIgSILENT 9
- 2.2 Electrical components models 9
 - 2.2.1 Cable model 9
 - 2.2.2 Transformer model 10
 - 2.2.3 Induction generator model 10

3 Detailed simulation model 11

- 3.1 General 11
- 3.2 Grid model 12
- 3.3 Wind turbine model 13
 - 3.3.1 Electrical model 13
 - 3.3.2 Mechanical model 14
 - 3.3.3 Aerodynamic model 16
 - 3.3.4 Control and protection system 17
- 3.4 Simulation outputs and data analyses 17

4 Simulation with idealised models 18

- 4.1 Description of idealised models 18
 - 4.1.1 Single line diagram 18
 - 4.1.2 Simulation time steps 19
- 4.2 Comparison of EMTDC and DIgSILENT basic models 19
 - 4.2.1 Short circuit comparison 19
 - 4.2.2 Steady state comparison 20
 - 4.2.3 Resonances above fundamental frequency 21
 - 4.2.4 Short circuit impedance definition 23
- 4.3 Influence of saturation models 23
- 4.4 Comparison of EMT and RMS models 24

5 Transient experiments 26

- 5.1 General 26
- 5.2 Selection of transient experiments 27
- 5.3 Measurement system 28
 - 5.3.1 Data acquisition system 28
 - 5.3.2 Wind turbine nacelle instrumentation 29
 - 5.3.3 Wind turbine 10 kV terminals instrumentation 29
 - 5.3.4 Substation 10 kV wind farm collection line instrumentation 30
- 5.4 Trip of one wind turbine at 10 kV terminal 30
 - 5.4.1 Description of experiment 30
 - 5.4.2 Measurement results 31
- 5.5 Trip of 10 kV wind farm collection cable at substation 36
 - 5.5.1 Description of experiment 36
 - 5.5.2 Measurement results 36
- 5.6 Emergency stop of one wind turbine 39
 - 5.6.1 Description of experiment 39
 - 5.6.2 Measurement results 39
- 5.7 Islanding of two wind turbines 43
 - 5.7.1 Description of experiment 43

5.7.2	Measurement results	44
5.8	Voltage change due to tripping	47
5.8.1	Description of experiment	47
5.8.2	Measurement results	47
5.9	Voltage change due to tap position changing	49
5.9.1	Description of experiment	49
5.9.2	Measurement results	50

6 Comparison of simulations and measurements 51

6.1	General	51
6.2	Trip of one wind turbine at 10 kV terminal	52
6.3	Trip of 10 kV wind farm collection cable at substation	57
6.4	Emergency stop	61
6.5	Islanding of two wind turbines	61
6.6	Voltage change due to tripping	64
6.7	Voltage change due to tap position changing	68

7 Conclusions 70

Appendix A Benchmark model 73

Preface

This report describes the results of the project titled “Simulation and verification of transient events in large wind power installations”. The project has been funded by the Danish Transmission System Operator, Elkraft System contract number Bro-91.054 (FU 1103), and it was carried out in cooperation between Risø National Laboratory, NVE HVDC-group, Aalborg University and NEG-Micon Control Systems.

1 Introduction

The objective of this work is to develop and verify tools, which can be used to study and improve the dynamic interaction between large wind farms and the power system to which they are connected. The background for this objective is the fast development of wind energy, with special focus on the challenges arising along with the offshore targets in Energy 21 [1] in Denmark. However, wind energy is becoming a significant supply in the power systems in many areas with good wind resources, and therefore wind energy will play an important role in the operation of these power systems. Thus, there is also a perspective for using the developed tools outside Denmark.

There are several technical aspects of this influence of wind energy on power systems where simulations with reliable tools can be of help to predict the impact of the wind energy development, and to improve the integration of the wind energy in the system. Three of these aspects are highlighted in the Danish Transmission System Operators specifications for connection of large wind farms to the transmission system [2], [3].

The first aspect to be mentioned is the influence of distributed generation on the local voltage quality. National standards / recommendations / requirements in this area have existed through more than a decade, and an IEC 61400-21 Final Draft International Standard on measurement and assessment of power quality of grid connected wind turbines [4] was issued in 2001. It includes the influence on steady state voltage as well as voltage fluctuations due to (active and reactive) power fluctuations of wind energy and harmonic distortion. These power quality issues are particularly relevant for systems where the wind energy development has taken place in rural areas, with grid connections based on the existing distribution grids in these areas.

The second aspect is the influence of (active and reactive) power fluctuations of wind energy installations on the control of the power systems. This is particularly relevant in smaller, isolated systems where the total penetration of wind energy in the system is high. However, also in strong interconnected systems this is becoming an issue when the wind energy penetration becomes significant in large areas of these systems. This is the case with the wind energy development in Denmark.

The third aspect is the transient behaviour of systems with wind energy in the event of grid faults. This becomes particularly relevant in cases where the wind energy production has become a significant part of the system production, and consequently the loss of a large part of the wind production in the event of grid faults can have severe consequences for the system stability.

The focus in this work is on the third aspect: the transient behaviour. But since the relevant models to simulate the three aspects have many things in common, it is also useful to relate to the other aspects.

A number of models for simulation of influence of wind farms on voltage quality have been developed, Estanquero et.al. [5] and Sørensen et.al.[6]. These models take into account the influence of turbulence and mechanical oscillations on the power fluctuations from wind farms. The influence of turbulence is decisively important in models of the power quality related to wind power fluctuations, but for the transient aspects, the wind models are not so important, because the transient events have a much stronger influence than the wind fluctuations on the system dynamics on the short term where the transients are interest-

ing. Still, the relevant dynamic models of wind turbines and grid are quite similar for transient simulation models and for simulation of voltage quality.

Also a number of models have been developed to simulate the behaviour of wind turbines in the event of grid faults. Akhmatov et.al. [7] showed that the traditionally used lumped mass models for dynamic simulations predict an unrealistically good stability of wind turbine induction generators and power system. It is therefore essential to include the mechanical oscillations in the wind turbine shaft in the model, using separate masses for turbine and generator. The shaft flexibility is also important for voltage quality models, because the shaft vibration amplifies the influence of wind fluctuations on power fluctuations for frequencies around the eigenfrequency determined by the rotor inertia and shaft flexibility.

The 12 MW wind farm installed in Hagesholm in Denmark has been selected as study case for the present project. The Hagesholm wind farm is shown in Figure 1. It consists of six NM 72/2000 wind turbines from NEG-Micon, with directly connected induction generators and active stall control of the blade angles.



Figure 1. Hagesholm wind farm consisting of 6 NM 72/2000 wind turbine. View is seen from S-SE.

The simulation models of the wind farm in this project are developed in the dedicated power analysis tools EMTDC and DIgSILENT. Comparing these two tools is interesting for several reasons.

EMTDC is a dedicated and well-established tool for simulations of transient or dynamic events – involving details with hundreds of components but typically less than ten rotating machines. EMTDC is however fast moving in the direction of including dedicated packages for analysis of dynamic stability and load flow / short circuit – including probably hundreds of rotating machines.

DIgSILENT is on the other hand a relative new tool but also evolving fast in the same direction - to include simulations of transient or dynamic events today. DIgSILENT was, however, born out of the load flow / short circuit community. This movement towards universal simulation tools is a general trend stressed by

the problems that planners of large electrical systems face these days and even more in the future.

During less than a decade most electrical systems in the western world have moved from including a few well-defined large machines integrated in a strong grid to a mixture of less or no large machines combined with many smaller machines. The latter typically at lower voltage levels with weaker grids and in the case of large wind farms with many small machines constantly influencing each other. This challenge calls for the universal simulation tools and is the reason for this trend.

So far only two simulation tools with all three packages (i.e. load flow, dynamic and transient simulations) are known to be well established: ABB's SIMPOW and Siemens' NETOMAC. So far and probably due to pricing they, however, do not seem well known in the wind power community, whereas DIgSILENT and EMTDC seem to gain foothold. This makes comparing EMTDC and DIgSILENT interesting.

In the present project, transient and dynamic cases with up to three rotating machines have been simulated with EMTDC and DIgSILENT. As both tools mature in the near future one might suggest comparing larger cases involving all the above mentioned packages. A technical description of the two tools is given in chapter 2.

Initial versions of the simulation models used in this project were already available at project start. The EMTDC model is based on the NVE model used in Christensen [8], whereas the DIgSILENT model is based on the Risø/AAU/Dancontrol model described in Sørensen et.al. [6].

The DIgSILENT model was originally developed for power quality analyses and run as an RMS model for that purpose, but since DIgSILENT is able to simulate with transient EMT models based on the same input data, which is used for RMS simulations, this is how the DIgSILENT model has been upgraded from an RMS model to an EMT model. The applied mechanical models are identical in the RMS and the EMT case.

Besides, both the EMTDC model and the DIgSILENT model have been extended with the protection and control features which are relevant for the behaviour of the wind turbines in the tested cases. However, the modelled protection and control is not described in details in this report, because the information is confidential.

The EMTDC model and DIgSILENT model applied in this project are quite similar, but some features are only available in one of the models. Chapter 3 describes the models, including information about where the models are different.

The models described in chapter 3 are denoted the "detailed simulation models" as they comprise the whole wind farm. In the following chapters, these full models are applied in reduced versions to fit specific purposes.

The first "reduced model" is the idealised models compared in chapter 4. Here the models are reduced to make the comparison between the different models more transparent. The idealised models are used to compare EMTDC and DIgSILENT, and to study the effect of saturation and electromagnetic transients. This is considered the first step to validate the models.

To provide further validation of the simulation models, measurements have been acquired in the wind farm and at the substation where the wind farm is connected. These measurements are described in chapter 5.

The validation of the models against measurements is the subject in chapter 6, where the measurements are compared to the simulations.

Finally, the conclusions of the work are outlined in chapter 7.

2 Simulation tools

2.1 Features of EMTDC and DIgSILENT

The simulation models of the wind farm used in this project are developed in the dedicated power system analyses tools EMTDC and DIgSILENT. These tools support simulations with full electromagnetic transient models (EMT), providing instantaneous values of voltages and currents in the grid, combined with the ability to build dynamic models for generator movers, which is in our case used to develop wind turbine models.

To build these models for generator movers, EMTDC includes in its standard library a multi-mass-model with up to five individual masses, corresponding spring constants, individual and mutual damping, output of all speeds torques etc. EMTDC allows the user to either rewrite the source code of an existing library model or freely build a new model with the users own graphics and source code. EMTDC is based on source code in Fortran.

In DIgSILENT, a library is also available, but it typically consists of more basic components. To implement primary mover models, the user can use DIgSILENT's own programming language DSL (Dynamic Simulation Language), which is also a combination of graphics and open source code.

Besides the EMT simulations, DIgSILENT provides the ability to make the so-called RMS simulations. These simulations are also referred to as (dynamic) stability simulations, and they correspond to standard models in other power system stability simulation tools, e.g. PSS/E. The advantage of using RMS simulations is that the simulation speed can be increased significantly, but the simulations omit the fast electromagnetic transients. The RMS simulations can be done with the symmetric component only or with the unsymmetric components as well. The stator transients in the induction generator models are omitted in the RMS-simulations, thus the order of the induction generator model is reduced. EMTDC does not have a similar feature.

DIgSILENT also provides the ability to either simulate with a fixed time step or a variable time step for the simulations. With variable time steps, DIgSILENT enables reduction of the simulation time increasing the simulation time steps to what is possible with respect to keep a stable simulation.

EMTDC provides the ability to include saturation in generator as well as transformer models. Both serial and shunt reactances can be modelled with saturation. DIgSILENT also supports modelling of saturation, but only in the transformers.

2.2 Electrical components models

2.2.1 Cable model

Figure 2 shows the single line diagram for the cable models used in EMTDC as well as DIgSILENT. It is seen that the model is a standard π equivalent. This model is available as standard component in DIgSILENT as well as EMTDC.

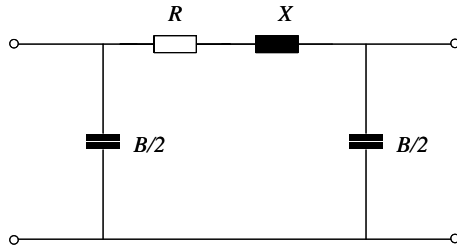


Figure 2. Single line diagram for cable

2.2.2 Transformer model

Figure 3 shows the single line diagram for the transformer models used in EMTDC as well as DIgSILENT. It is seen that the model is a standard T equivalent. This model is available as standard component in DIgSILENT as well as EMTDC.

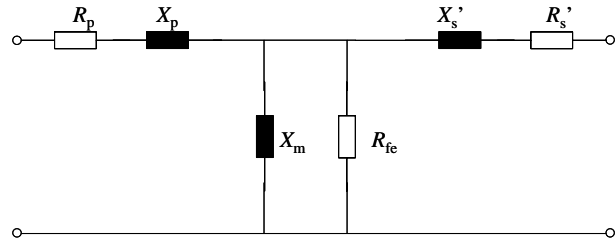


Figure 3. Single line diagram for transformer model

2.2.3 Induction generator model

Both EMTDC and DIgSILENT provide models for induction generators. In the present project, we have selected a model, which can be implemented in both tools as a reduction of the build-in models, and we have applied the same parameters in both models.

The steady state equivalent for the DIgSILENTs library models of induction machines is shown in Figure 4. It consists of a general model for the stator, which can be combined with three different rotor models, depending on the type of generator.

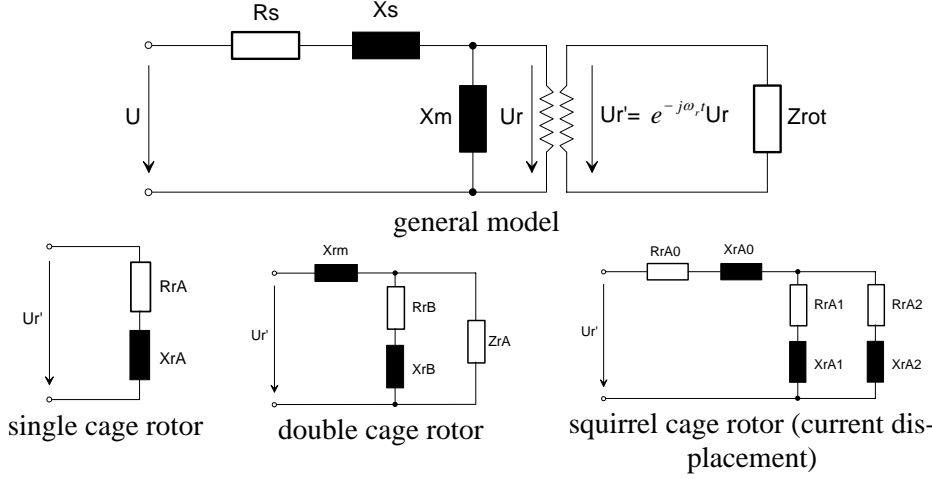


Figure 4. Steady state single line equivalent of induction machine models in DIgSILENT PowerFactory. Source: Digsilent note on induction machine models [9].

In EMTDC, there is one universal model for squirrel cage induction machines. Figure 5 shows the steady state single line equivalent of the EMTDC induction machine model. X_s , X_{r0} and X_m can be modeled as fixed or saturable. In the latter case one can freely input any saturation curve. EMTDC includes a very identical universal model for the doubly fed induction machine with full access to all 6 phases. It was, however, not needed in this case.

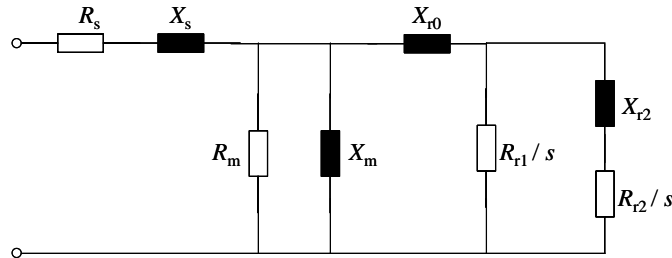


Figure 5. Steady state single line equivalent of the EMTDC squirrel cage induction machine.

3 Detailed simulation model

3.1 General

In this section, the detailed gross model of the Hagesholm wind farm including its grid connection is described. For comparisons of simulations in chapter 4, and for comparison between measurements and simulations in chapter 6, this gross model is reduced to only include the relevant parts in the individual cases.

3.2 Grid model

The grid collecting the power from the wind farm is shown in Figure 6. The substation has two transformers and a double busbar system. The wind turbines are connected to the substation through two collection lines. A backup line is also available between the ends of the two collection lines.

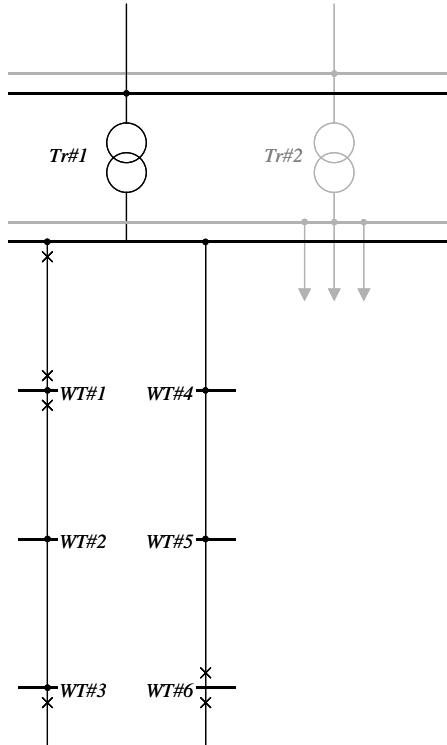


Figure 6: Grid model for the connection of the Hagesholm wind farm.

As indicated in Figure 6, the two transformers and the double busbar system in the 50/10 kV substation are utilised to isolate the wind farm on transformer #1. The loads are supplied by their own transformer #2. Also, the transformers are fed by different parts of the 50 kV grid. This coupling ensures a minimum of disturbance of the consumers due to the experiments, and it limits the relevant modelling to the black parts of Figure 6, whereas the grey parts are omitted from the models. Actually, as a consequence of the selection of experiments, it has only been necessary to model the NVE owned wind turbines #1, #2, and #6.

A large number of breakers are also available in the grid. Figure 6 indicates the 10 kV breakers that are used in the experiments and simulations presented in this report.

The substation transformers have on-line automatic tap changers to control the 10 kV voltage. In the present models, the tap positions are assumed to be fixed because they are not expected to change during the short periods where the transients are studied, except in an experiment where the taps are manually changed to provide a voltage step.

The 50 kV grid is simply modelled by a Thevenin equivalent. This is a reasonable approximation for modelling of grid faults in the 10 kV grid, because the 50 kV grid is relatively strong.

3.3 Wind turbine model

A dynamic wind turbine model is connected to each of the wind turbine terminals in Figure 6. Each wind turbine is modelled individually, providing a realistic model for the dynamics of the wind farm.

The model of an individual wind turbine is shown in Figure 7. It includes an electric part, a mechanical part and an aerodynamic part, and a part representing the control system. The control system model provides the blade pitch angle θ_{pitch} for aerodynamic model, including the control in the event of a grid fault. Besides the pitch angle, the aerodynamic part is driven by the wind speed u , which will be set to a constant for the initial simulations of transient events.

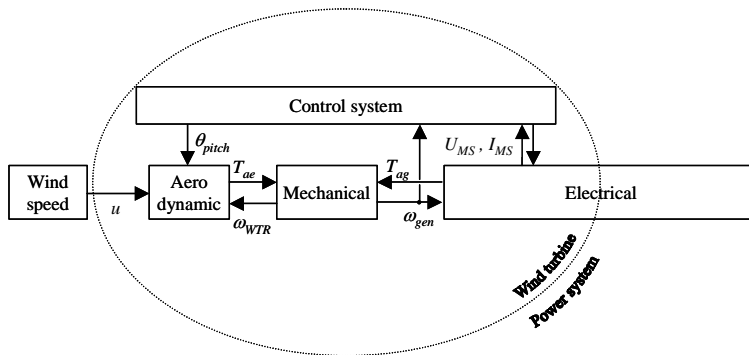


Figure 7: Wind turbine model with interface to power system (grid) model and wind speed model.

Inputs to the model of the wind turbine control system are the voltage U_{MS} , current I_{MS} measured by the control system at the main switch, in addition to the generator speed ω_{gen} . Besides the pitch angle, the outputs from the control block are control signals indicating when the contactors at the generators and capacitors should be opened.

3.3.1 Electrical model

The electrical part of the wind turbine model is shown in Figure 8. It includes induction generator, capacitor banks for reactive power compensation and the step-up transformer. The transformer is placed in the nacelle, and the 10 kV cable through the tower is included in the model. Finally, the contactors for disconnection of generator and capacitor are included.

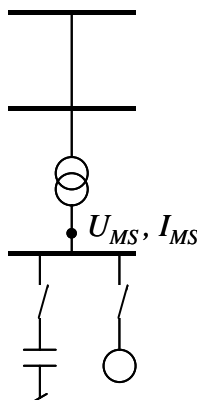


Figure 8: Model of the electrical part of the wind turbine.

The softstarter and the small generator are not included in the models, because only transients not involving the softstarter and small generator have been studied. Besides, the wind turbines are equipped with an auxiliary transformer for supply, which is also not included in the model because it is relatively small. Likewise, the hydraulic pump for the pitch system is not included.

Note that U_{MS} and I_{MS} in the model diagram in Figure 7 are taken from the low voltage side of the step-up transformer, corresponding to the electrical point where the actual control system measures voltage and current on the main switch.

The capacitor bank actually consists of 10 steps, but it is modelled here as a single step because they are assumed to be switched off simultaneously during the transient events.

Figure 9 shows the single line equivalent of the induction generator model used for the present simulations in EMTDC as well as DIgSILENT. The model is implemented as a reduced version of the universal model of a squirrel cage induction generator in Figure 5, and as a reduced version of the DIgSILENT model with squirrel-cage rotor in Figure 4. Basically, the selected model is the EMTDC model without iron losses, because iron losses are not available in DIgSILENT. The steady state model is used in the initial load flow, which is performed before any dynamic simulation (RMS or EMT) in DIgSILENT, and besides the steady state model provides the input parameters for the transient model, which is a d-q-0 model.

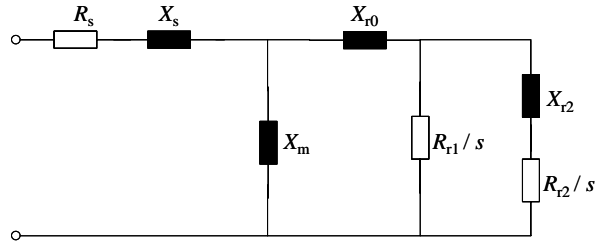


Figure 9: Steady state single line equivalent of induction generator.

The parameters for the model have been estimated by NVE based on the generator test reports provided by NEG-Micon Control Systems. The method applied to estimate the parameters is a compromise between fitting of active and reactive power, slip and torque in a number of working points where the test report provides data. It is not possible to make an exact match to all the data applying the model in Figure 9, so the estimated parameters are a compromise, where high priority has been given to the torque / slip relation. Thus, some differences are expected between tested and modelled relation between active and reactive power. The steady state model is used in the initial load flow, which is performed before transient simulation, and besides the steady state model provides the input parameters for the transient model like in DIgSILENT.

3.3.2 Mechanical model

The mechanical model of the wind turbine is shown in Figure 10. It is essentially a two mass model connected by a flexible shaft characterised by a stiffness k_{ms} and a damping c_{ms} . Moreover, an ideal gear with the exchange ratio $1:f$ is included.

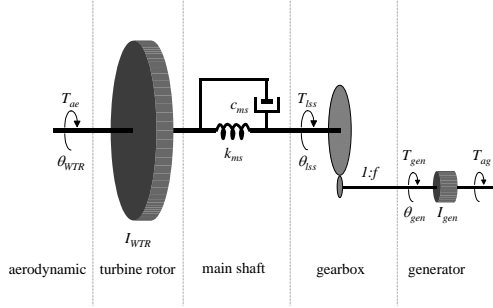


Figure 10: Model of the mechanical part of the wind turbine.

The masses used in this model correspond to a large turbine rotor inertia I_{WTR} representing the blades and hub, and a small inertia I_{gen} representing the induction generator. The generator inertia is actually included in the generator model, specified as an inertia time constant. The two-mass model is in accordance with the recommendations of Akhmatov et.al. [7].

The stiffness and damping components are modelled on the low speed shaft, but flexibility in the gearbox and on the high speed shaft can also be included here, if they are corrected for the gear ratio.

More complex mechanical models can also be suggested. One suggestion could be to detail the drive train model. Another suggestion could be to include more parts of the wind turbine flexibility in the model.

One way to detail the drive train model would be to include backlash. Backlash is normally not included when the model simulates continuous operation of the wind turbine, because the torque remains positive when the wind speed is above cut-in wind speed. However, if the generator is tripped, the torque will oscillate between positive and negative values, and then the backlash will become visible.

Another suggestion to detail the drive train model is to apply a third mass representing the gearbox as suggested by Iov [10] (and possibly brake disc) and include the flexibility on the high speed shaft separately.

However, the advantage of the present drive train model is that the uncertain parameters can be estimated or verified by measuring the shaft torque when the generator is tripped. Normally, the inertias and gear ratio in the model will be known with very high precision, while the stiffness and damping are much more uncertain. When the generator is tripped, the model can be reduced to a single eigenfrequency represented by the stiffness k_{ms} , the damping c_{ms} and the equivalent inertia I_{eq} determined by

$$I_{eq} = \frac{I_{WTR} \cdot f^2 I_{gen}}{I_{WTR} + f^2 I_{gen}} \quad (1)$$

The equivalent is shown in Figure 11. If $f^2 I_{gen} \ll I_{WTR}$, the mode can be understood as the small inertia $f^2 I_{gen}$ oscillating against the wall I_{WTR} .

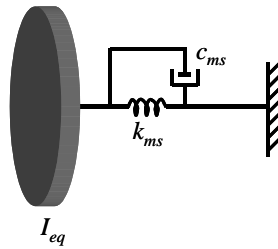


Figure 11: Equivalent mechanical model when the generator is tripped.

In this case, the stiffness can be estimated by the eigenfrequency f_{osc} of the oscillation according to

$$k_{ms} \cong (2\pi f_{osc})^2 I_{eq} \quad (2)$$

while the damping can be estimated by the logarithmic decrement δ_{eq} of the oscillation according to

$$c_{ms} = 2 \cdot \delta_{eq} \cdot \sqrt{\frac{k_{ms} \cdot I_{WTR}}{\delta_{eq}^2 + 4\pi^2}} \cong \frac{\delta_{eq}}{\pi} \cdot \sqrt{k_{ms} \cdot I_{WTR}} \quad (3)$$

When the model was designed, it was assumed that only the drive train would have a significant influence on the dynamics of the interaction with the grid. Since then, studies by Larsen et.al. [11] with a combination of a detailed aeroelastic model and a dynamic generator model have shown that the second sideways tower bending mode can couple with the generator eigenfrequency and thus cause a substantial increase in the generator power fluctuation as well as the tower vibration. It would also be an option for future transient models to include this tower flexibility.

As DIgSILENT does not include a standard library model of a multi-mass-system like the above mentioned, this has been programmed by the user in the dynamic simulation language DSL. For the EMTDC model, the multi-mass-model in its standard library has been used to implement the present two mass model.

3.3.3 Aerodynamic model

The aerodynamic model was originally based on tables with the aerodynamic efficiency C_p , i.e.

$$P_{ae} = \frac{1}{2} \rho A u^3 C_p \quad (4)$$

where ρ is the air density, A is the swept area, u is the wind speed and $C_p = C_p(\lambda, \theta_{pitch})$ is the aerodynamic efficiency, which depends on the tip speed ratio λ and the blade pitch angle θ_{pitch} . The tip speed ratio λ is defined as

$$\lambda = \frac{\omega R}{u} \quad (5)$$

where R is the radius of the aerodynamic rotor. This is a quasi static aerodynamic model which determines the output aerodynamic torque M_{ae} directly from the input wind speed according to

$$M_{ae} = \frac{P_{ae}}{\omega} = \frac{1}{2\omega} \rho A u^3 C_p \quad (6)$$

However, since C_p must be infinite to provide a starting torque when $\omega = 0$, the model has been adjusted so that a C_q table replaces the C_p table, and (6) is replaced by

$$M_{ae} = \frac{1}{2} \rho A R u^2 C_q = \frac{1}{2} \rho \pi R^3 u^2 C_q \quad (7)$$

The DIgSILENT model can include a model for dynamic stall. The implemented model for dynamic stall is based on Øye's dynamic stall model [12], simulating dynamic stall as time lag of separation. Øye implements the time lag directly on the lift coefficients in the individual blade sectors, but this is not possible in our case, because we base the aerodynamic calculations on C_p .

Dynamic stall could also be relevant for modelling of transient behaviour at high wind speeds, i.e. above 13 m/s. Also dynamic inflow is shown to have a significant influence when the pitch angle is changed very fast [13], which is often the case during transient events.

However, to keep the models simple in the first place, and to ease the comparison between the DIgSILENT model and the EMTDC model, only quasi static aerodynamic models have been used in this project.

The EMTDC model uses a standard library model to input the C_q table as function of pitch angle and tip speed ratio. The model allows real time interpolation of practically any number of data points. To keep the simulation time down around 200 data points were chosen for each turbine.

In DIgSILENT, also a standard table is used to input the C_q table, but in the DIgSILENT model the table is more detailed, using 10000 data points. The effect of the size of the C_q table on the simulation time of the DIgSILENT model has not been studied.

3.3.4 Control and protection system

The control and protection system response to abnormalities is essential to model to obtain realistic simulation results of the behaviour of the wind turbines during and after transient events.

The response, which is included in the present models, is the detection of the abnormal conditions and the succeeding pitch and contactor response. The abnormal condition can be a registered as a grid fault, or as an overspeed if this occurs before the grid parameters exceed their limits.

The EMTDC model uses standard library models to simulate the control and protection system.

3.4 Simulation outputs and data analyses

To compare the simulation results, which are simulated with different models, and to compare simulations to measurements, a number of quantities have been selected. Some are simulated / measured directly, while other parameters are derived from the directly measured / simulated quantities.

On the mechanical side, we compare rotor speeds and torques. The compared rotor speeds are the low speeds on the blade rotor and the high speeds on the generator rotor. These are simulated and measured directly.

The simulated torques are the aerodynamic torque and the generator torque, while the measured torque is the torque on the low speed shaft. To compare the measured torque to simulations, we simply use the simulated angle difference $\theta_{WTR} - \theta_{ls}$ to calculate the simulated shaft torque T_{lss} according to

$$T_{lss} \cong k_{ms} \cdot (\theta_{WTR} - \theta_{ls}) \quad (8)$$

On the electrical side, we simulate and measure instantaneous values of currents and voltages directly. Converting all measured currents to line currents and all voltages to line voltages, these are directly comparable to the corresponding simulated values.

Besides the voltages and currents, active and reactive power is also compared. The simulation tools have build-in methods to calculate active and reactive power, but to ensure transparency and to enable comparisons to measurements, the instantaneous active power $p(t)$ is simply calculated as

$$p(t) = \sum_{i=1}^3 u_i(t) \cdot i_i(t) \quad (9)$$

where u_i is line-to-neutral voltage of line i and i_i is line current of line i . Similarly, the instantaneous reactive power $q(t)$ is calculated as

$$q(t) = (u_1(t) - u_3(t)) \cdot i_1(t) + (u_2(t) - u_1(t)) \cdot i_2(t) + (u_3(t) - u_1(t)) \cdot i_3(t) \quad (10)$$

which is formally only valid for the fundamental components of currents and voltages, but provides an informative and convenient *instantaneous* expression for the reactive power.

Finally, we will sometimes plot the fundamental components of voltages and currents, and the corresponding fundamental frequency. That data is obtained from Risøs power quality analyses software package, which fits the (measured or simulated) instantaneous values of e.g. a voltage to provide the RMS value, phase angle and frequency of the signal voltage in each line period. The power quality software package also provides the positive sequence of voltages and currents, based on the fundamental components of all three phases.

4 Simulation with idealised models

4.1 Description of idealised models

The idealised models are reduced versions of the detailed model described in chapter 3. The models are reduced in order to make the comparison between the different models more transparent. The idealised models are used to compare EMTDC and DIgSILENT, and to study the effect of saturation and electromagnetic transients.

4.1.1 Single line diagram

Figure 12 shows the single line diagram of the idealised models. It includes the 50 kV grid G_{50} as a Thevenin equivalent, the transformer T_{Gr} being identical to Tr#1 in Figure 6, the wind farm collection cable Ca_{Col} , being identical to the cable to wind turbine #1, the tower cable Ca_{Tow} , in the wind turbine, the nacelle transformer T_{WT1} , the reactive power compensation capacitor C_{WT1} and the high speed induction generator G_{WT1} .

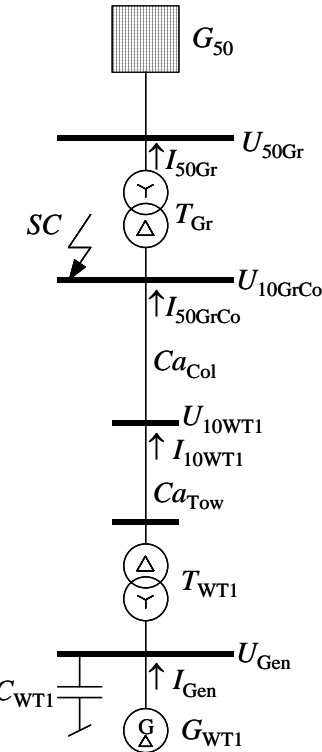


Figure 12: Single line diagram of the idealised model

4.1.2 Simulation time steps

For the simulations presented in this chapter, the simulation time steps have been held constant. This has been done to focus the comparison between EMTDC and DIgSILENT on the dynamics of the models in the first place rather than on the variable time step feature in DIgSILENT. The constant simulation time step has been selected to $10 \mu\text{s}$. This is sufficiently small to ensure stable simulation of the generator dynamics as seen in the following, and also a higher eigenfrequency (approximately 3 kHz) caused by the capacity in the collection cable can be simulated with this option.

The simulation results have been saved and shown in graphs only with $100 \mu\text{s}$ time step size. This corresponds to a 10 times reduction of the data before it is saved. This reduction has been done to minimise the amount of data, and it can be justified because frequencies above 5 kHz do not occur in the simulations.

4.2 Comparison of EMTDC and DIgSILENT basic models

4.2.1 Short circuit comparison

Figure 13 and Figure 14 show the simulated voltages and currents in the generator during the short circuit. The short circuit is activated at time $t = 0$ and cleared at time $t = 0.1 \text{ s}$. The simulations include electromagnetic transients in the models, but saturation is not included.

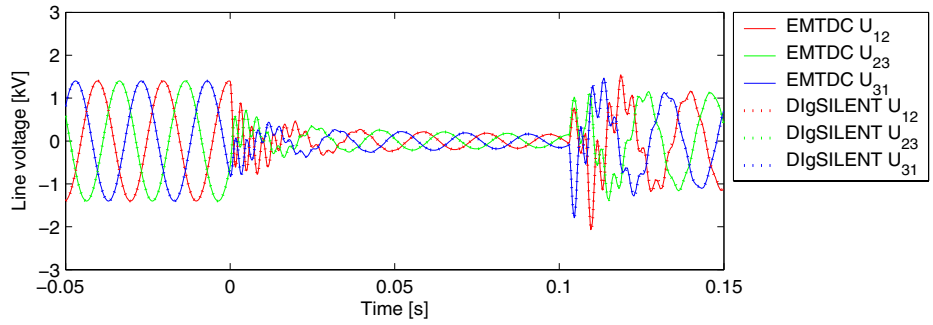


Figure 13: Simulated generator voltages with EMTDC and DIgSILENT

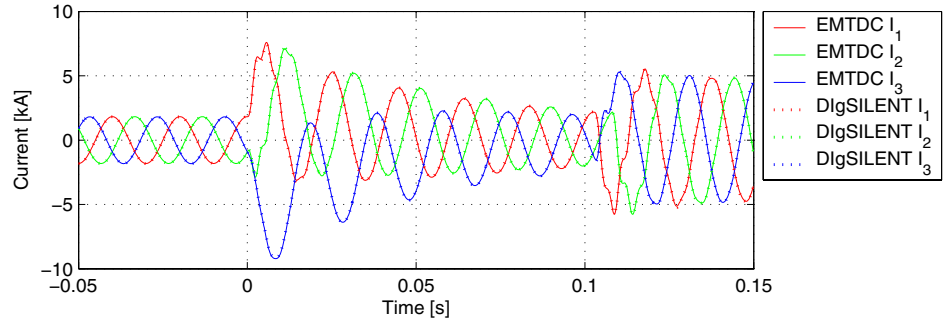


Figure 14: Simulated generator currents with EMTDC and DIgSILENT

The figures first of all show a very close agreement between the EMTDC and DIgSILENT simulations of voltages and currents. The graphs have been generated using thin full lines for the EMTDC simulations and thicker dotted lines for the DIgSILENT simulations. It is generally seen that the thin full lines coincide with the corresponding thick dotted lines, i.e. that the agreement between DIgSILENT and EMTDC is very good.

4.2.2 Steady state comparison

However, looking closer at the steady state 100 ms before the short circuit, it is observed that the generator torque is constant in the DIgSILENT simulation, while it has a significant sinusoidal variation in the EMTDC simulation as shown in Figure 15.

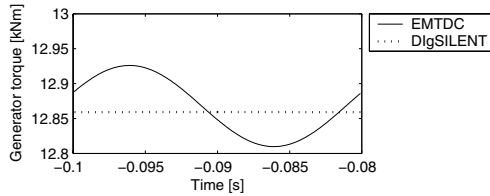


Figure 15: Simulated generator torque in steady state before the short circuit

The reason for the sinusoidal variation in EMTDC has been investigated. First of all, a similar variation is seen in the instantaneous power, which indicates that DC-components in voltages and/or currents could be the explanation.

Calculations on voltages and currents in the steady state show that the DC-components in the voltages are very small, but the line currents have DC-components which are 0.3-0.6 % of the fundamental component of the line current.

If we removed the DC-components from the line currents, the calculated instantaneous power in steady state becomes constant. Thus, the observed sinusoidal variation in power and torque is due to DC-components in the line currents. The reason for the current DC-components has not been identified.

4.2.3 Resonances above fundamental frequency

Figure 13 shows that the generator 960 V line-to-line voltages contain significant oscillations with frequencies above the 50 Hz fundamental frequency. The oscillations are excited by the activation of the short circuit and by the clearing of the short circuit. The oscillations can also be seen in the currents in Figure 14, but they are most significant in the voltages. It is also seen that the high-frequency oscillations are strongly damped and disappear after a few line periods.

The eigenfrequencies of the oscillations have been identified applying the reduced equivalent diagram of the simulation model shown in Figure 16. The sections indicated in Figure 16 corresponds to the grid, with the same labels as were used in the single line diagram Figure 12, i.e. G_{50} represents the 50 kV grid, T_{Gr} is the transformer in Grevinge, Ca_{Col} is the power collection cable, Ca_{Tow} is the tower cable, T_{WT1} is the nacelle transformer, C_{WT1} is the capacitor bank and G_{WT1} is the induction generator.

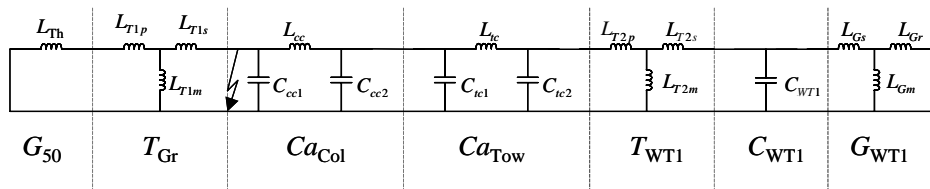


Figure 16: Reduced single line diagram for the total simulation model.

The reduction to the equivalent in Figure 16 has first of all been obtained by replacing all resistances by short circuits, assuming that the eigenfrequencies are mainly determined by the capacities and the inductances. Thus, the values of the parameters can be taken almost directly from the corresponding component models. As an example, for the generator model, we have calculated L_{Gs} in

Figure 16 from X_s in Figure 9, L_{Gm} from X_m and L_{Gr} from X_{r0} , all assuming 50 Hz.

For an oscillatory circuit with a capacitor C looking into the inductance L , the eigenfrequency f can be determined according to

$$f = \frac{1}{2\pi\sqrt{LC}} \quad (11)$$

During the short circuit (indicated in Figure 16), the capacitor $C=C_{WTI}$ approximately looks into the inductance $L=(L_{T2s}+L_{T2p}+L_{tc} + L_{cc}) \parallel (L_{Gs}+L_{Gr})$. Seen from C_{WTI} , the other capacitors can be discarded because they are decays lower than C_{WTI} , and the shunt inductances L_{T2m} and L_{Gm} can be discarded because they are decays higher than the serial inductances. Inserting these values for C and L in ((6)), an eigenfrequency $f=302$ Hz is found, which corresponds very well to the oscillation frequency in the first line periods of the short circuit shown in Figure 17.

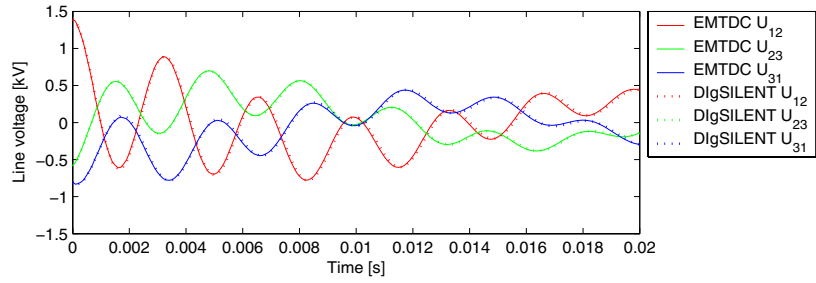


Figure 17: Simulated generator voltages with EMTDC and DIgSILENT in first line period of the short circuit.

With the short circuit cleared, the capacitor $C=C_{WTI}$ approximately looks into the inductance $L=(L_{T2s}+L_{T2p}+L_{tc} + L_{cc} + L_{T1s}+L_{T1p}+L_{Th}) \parallel (L_{Gs}+L_{Gr})$. Inserting these values for C and L in ((6)), an eigenfrequency $f=280$ Hz is found, which corresponds very well to the oscillation frequency in the first line period after the short circuit is cleared at $t = 0.1$ s, as shown in Figure 18.

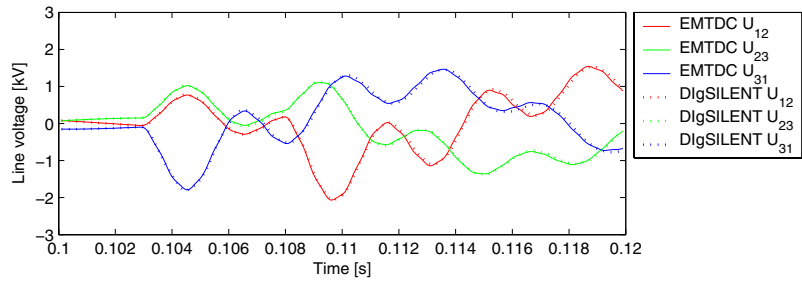


Figure 18: Simulated generator voltages with EMTDC and DIgSILENT in first line period after the short circuit is cleared.

4.2.4 Short circuit impedance definition

Another aspect, which has been identified as a result of the comparisons, is that the definition of the short circuit impedance is different in the two programs. In DIgSILENT, the impedance of a three-phase short circuit is interpreted as the impedance from phase to neutral in a star connection, whereas in EMTDC the corresponding short circuit impedance is interpreted as the impedance of each branch in a delta connection. Thus, there is a factor 3 between the input short circuit impedances in the two programs if they should be equivalent.

This difference does not have much influence on the fundamental components of voltages and currents if the short circuit impedances are very small, but the damping of the eigenfrequencies is strongly affected by the size of the short circuit resistances.

4.3 Influence of saturation models

Saturation models are available for transformers and generators in EMTDC. In the present version of DIgSILENT, saturation models are available for the transformers, but not for the induction generators. To assess the effect of saturation in the models, we have made an EMTDC simulation including saturation in generator and transformers, and compared it to the EMTDC simulation without any saturation.

The simulation results with and without saturation deviate some in the transient instants. Figure 19 and Figure 20 shows the line voltages and line currents during the short circuit. It is seen that the most significant difference is in the line currents. The peak line current in the first line period of the short circuit ($t = 0 - 0.02$ s) is underestimated with approximately 10 % without saturation, while the line current in the first line period after short circuit ($t = 0.1 - 0.12$ s) is slightly overestimated without saturation.

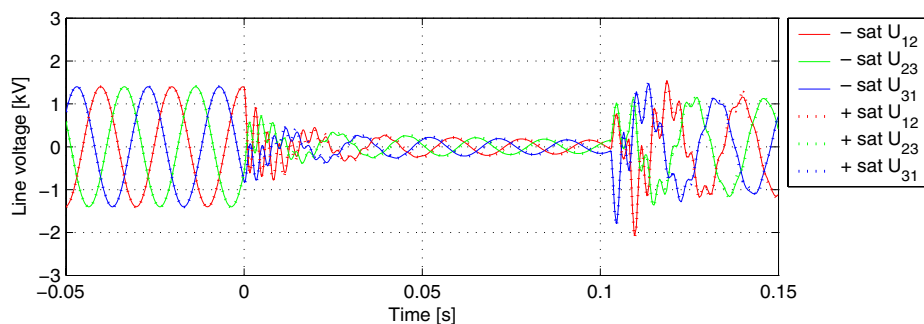


Figure 19: Generator line voltages during short circuit, simulated with EMTDC, without and with saturation effects in the models.

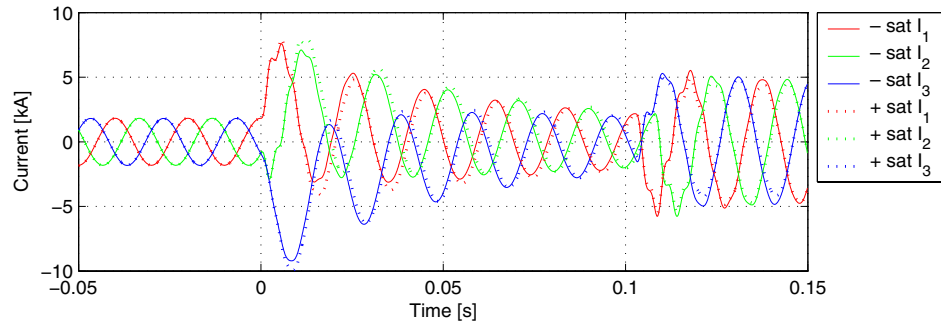


Figure 20: Generator line currents during short circuit, simulated with EMTDC, without and with saturation effects in the models.

4.4 Comparison of EMT and RMS models

In addition to the transient EMT simulations, DIgSILENT provides an option for so-called RMS simulations. In the RMS case, the system is simulated in the positive, negative and zero sequences, with the possibility to include only positive sequence in symmetric cases. In the present case, we simulate a symmetric fault, and therefore only the positive sequence is simulated.

The advantage of using an RMS simulation is that the simulation time is significantly reduced compared to an EMT simulation. The increased simulation speed makes it possible to simulate much longer events and much more complex systems.

Figure 21 shows the simulated generator torque during the short circuit with EMT and RMS options respectively. It is clearly seen that the RMS simulations strongly underestimate the variations in the generator torque by excluding the fundamental frequency (50 Hz) oscillations.

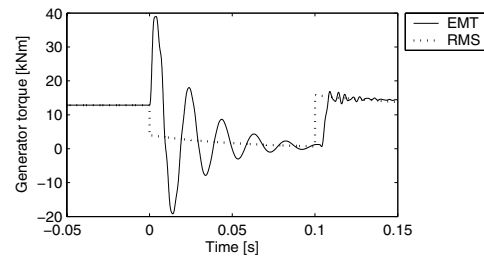


Figure 21: Simulated generator torque with DIgSILENT EMT and RMS options respectively.

The 50 Hz oscillations are due to the stator flux transients, which are commonly neglected for dynamic power system stability studies [14].

Akhmatov has studied the influence of the stator flux transients [15] on wind turbines with double-fed induction generators. Akhmatov concludes that the discrepancies between the simulated electric properties with and without stator

flux transients are important if fast over-current protection e.g. of power converters is considered, but otherwise it is more of academic interest.

Figure 22 and Figure 23 show voltage and current simulated with EMT and RMS options. To enable the comparison of the instantaneous values simulated with the EMT option to the vector magnitudes simulated with the RMS option, the RMS values of the EMT simulation have been calculated as root-mean-square with a half line-period (10 ms) averaging time.

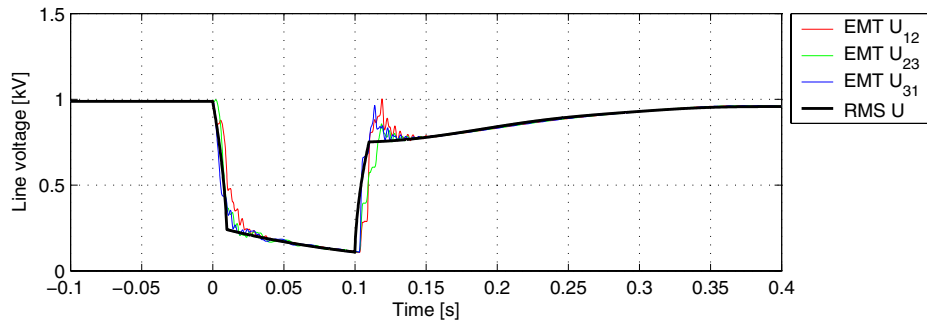


Figure 22: Simulated generator line-to-neutral voltage with DIGSILENT EMT and RMS options respectively.

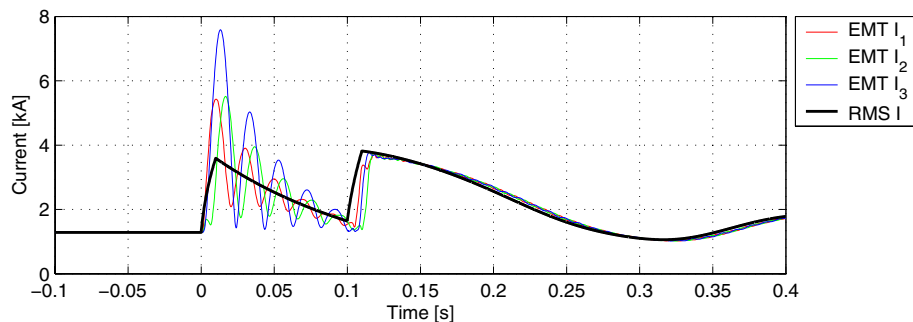


Figure 23: Simulated generator line current with DIGSILENT EMT and RMS options respectively.

It is seen in Figure 23 that the current transients caused by the short circuit are very high, but also very strongly damped. Therefore, the discrepancies between DIGSILENT EMT and RMS simulations are relevant when fast protection equipment is considered in the simulations, which is often the case for power converter protection as mentioned by Akhmatov.

Another important observation is that the behaviour after the short circuit is the same with the RMS and EMT simulations, which of course only is the case because no protection relays are tripped by the fast transients. If no fast relays are tripped, the long-term stability of the system is not affected by the stator flux transients, and consequently the dynamic system stability can be studied using the RMS simulations. As mentioned above, this is relevant for the simulation time, because even though computer speeds increase, there is also a need to

simulate the stability of very complex power systems with a reasonable representation of the distributed generation.

The influence of generator dynamics on mechanical loads on wind turbines has been studied by Larsen et.al. [11]. Simulations with advanced aeroelastic tools using induction generator models with and without stator flux transients have shown that these transients have very little influence on the mechanical loads on the wind turbine.

This is confirmed by the present simulations in DIGSILENT. Figure 24 shows the simulated shaft torque until 4 seconds after the short circuit with EMT and RMS options respectively. It is seen that the mechanical shaft torque is predicted very well with the reduced RMS model. This again confirms that the longer term dynamic stability of the power system is not affected by the stator flux transients, provided that no relays are tripped by the transients.

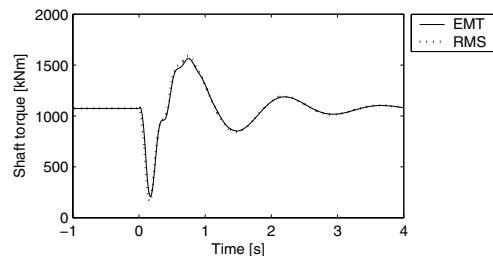


Figure 24: Simulated shaft torque with DIGSILENT EMT and RMS options respectively.

5 Transient experiments

5.1 General

In this chapter, we will describe the selection of the transient experiments, the measurement system, and for each of the selected transient experiments, we will describe the experimental setup and provide the main measurement results.

The selection of transient experiments is described in section 5.2. The purpose of the transient experiments is to support validation of the simulation models. Since the ultimate purpose of the models is to be able to simulate and improve the behaviour of large wind farm installations in abnormal grid conditions, mainly in the event of grid faults, it would be obvious to make a grid fault experiment. However, the risk to worsen the power quality of the consumers, and the risk to damage equipment has precluded that experiment. Instead, a number of less risky transient experiments have been selected.

The measurement system is described in section 5.3. It provides mechanical (drive train) measurements as well as electrical measurements. The measurement system consists of 3 identical datalogging systems, which have been moved around in the grid depending on which electrical measurement points were most interesting for the individual experiments.

The selected experiments including experimental setup and measurement results are described in sections 5.4 - 5.9.

5.2 Selection of transient experiments

The basic idea with the transient events is to generate disturbance in the grid in order to observe how this affects a wind turbine under operation. The disturbances can be caused by existing equipment or by installation of special equipment.

The following transients experiments have been considered:

1. Trip of one wind turbine.
2. Simultaneous trips of five wind turbines.
3. Trip of one wind farm line.
4. Switch-on of one wind turbine generator.
5. Simultaneous switch-ons of five wind turbine generators.
6. Switch-on of one generator without softstarter.
7. Simultaneous switching of all capacitors in one wind turbine.
8. Simultaneous switching of all capacitors in five wind turbines.
9. Switching of 50/10 kV transformer on secondary side.
10. Manual tap changing of 50/10 kV transformer ($\pm 7\cdot2\%$)
11. 2 phase short circuit on isolated 10 kV overhead line using piano string.
12. Interruption of 50/10 kV transformer for 50 ms on primary side.

Special attention has been paid to the possibility to make a short circuit, because the main purpose of the models is to enable simulations of short circuits. However, the risk to influence the consumer power quality and the risk to damage equipment has precluded the implementation of a short circuit experiment.

Instead of short circuits, less risky transient experiments have been selected. The selected experiments are:

1. Trip of one wind turbine at 10 kV terminal
2. Trip of 10 kV wind farm collection cable at substation
3. Emergency stop of one wind turbine
4. Islanding of two wind turbines
5. Voltage change due to tripping
6. Voltage change due to tap position changing

These experiments excite the wind power installation in different ways, which are useful to validate the models.

The first two experiments are quite similar: one wind turbine is tripped by opening a breaker in the 10 kV grid, and the wind turbine will shut down when the wind turbine control and/or protection systems respond to the observed fault conditions.

The emergency stop is an immediate stop of a wind turbine, which is available for safety reasons.

The next two experiments, the islanding of two wind turbines and the voltage change due to tripping are actually identical experiments. Two wind turbines are tripped, and the wind turbines will be shut down. However, the experiment has been made twice, and the measurement equipment has been moved from one experiment to the other. In the islanding experiment, the measurements are performed on the island, i.e. on the two tripped wind turbines. In the voltage change experiment, the focus is on the response of a wind turbine, which stays on the grid. This wind turbine will experience a transient voltage change on the grid due to the tripping.

Finally, another voltage change has been made by manually changing the tap positions of the transformer in the substation. This also provides measurements of the response of a wind turbine, which stays on the grid.

5.3 Measurement system

5.3.1 Data acquisition system

The data acquisition is based on 3 almost identical data acquisition systems. The systems are installed at different points of the grid, and are not interconnected. Thus, the 3 data acquisition systems log data asynchronously.

One of the data acquisition systems is illustrated in Figure 25. It consists of a laptop equipped with an analogue to digital converter (ADC) dedicated fast measurements of 3 phase voltages and currents. The ADC gets its analogue input signals through a signal conditioning equipment providing filtering, amplification of the external input signals to the input range of the ADC, and simultaneous sampling of the filtered and amplified signals. In addition, one of the three data acquisition systems uses the standard RS-232 serial input port of the laptop to log slower sampled mechanical data. The serial data is provided by a data acquisition unit (DAU), which converts the analogue mechanical measurement signals to serial input standard.

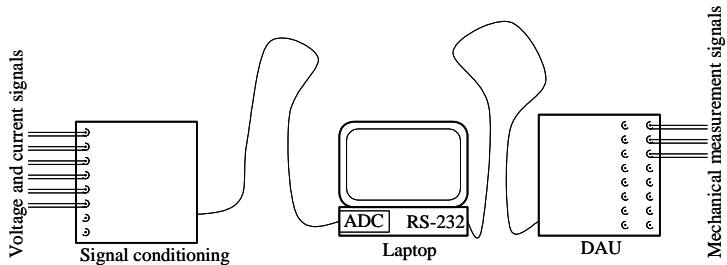


Figure 25. The data acquisition system

The laptop is a 1 GHz IBM ThinkPad with 128 MB RAM and a 28.6 GB HD.

The ACD card is a AI-16E-4 from National Instruments. The maximum sampling rate is 500 kS/s. The ADC card is inserted directly in the PCM-CIA slot of the laptop.

The signal conditioning unit is joined in the National Instrument SCXI-1000 chassis with 4 slots for SCXI cards. Only 2 slots are used in the present system.

The voltage and current sensor signals are connected through a SCXI-1305 BNC terminal block, in the ranges $\leq \pm 5$ V.

The terminal block is connected to the front of a SCXI-1141 8 channel elliptic lowpass filter block, which occupies the first slot in the SCXI-1000 chassis. The SCXI-1141 is equipped with programmable cut-off frequency and programmable individual gains of the channels. The cut-off frequency of the filters can be programmed to frequencies from 10 Hz to 25 kHz, with available values $f_c = 100 \text{ kHz} / n$ where n is an integer. The individual channel gain makes it possible to adapt the voltage level of the input signals to the ± 5 V of the ADC and thus minimise the discretisation noise of the ADC. The maximum gain is 100, i.e full range of the ADC can be obtained with ± 50 mV input signal, corresponding to $100 \text{ mV} / 2^{12} = 24 \mu\text{V}$ step size.

The SCXI-1141 filter block is then connected to a SCXI-1140 8 channel simultaneous sampling 8 channel differential amplifier block, which occupies the second slot in the SCXI-1000 chassis. The simultaneous sampling block sends the multiplexed signals via the SCXI bus to the first channel in the ADC in the laptop.

The DAU unit is a standard Risø unit, which has been developed for meteorological measurements and for wind turbine performance and mechanical load measurements. It provides serial output with a fixed sampling frequency of 35 Hz, which is sufficient for the present mechanical measurements. On the input

side, each analogue input channel can be selected as either a continuous analogue signal or as a pulse. The continuous analogue channels are simply sampled with 35 Hz. For the pulse channels, the time between each pulse is determined as the number of clock pulses of an internal 16 kHz clock. This is useful for wind speed measurements with anemometers as well as for rotor speed measurements.

Risøs LQ software developed in Labview controls the measurement hardware and acquires the data to the harddisk of the Laptop. It supports simultaneous data logging from the ADC and the serial port, although the ADC and DAU measurements are not synchronized. The sampling frequency of the ADC is set to 10 kHz, and the cut-off frequency 3 kHz.

5.3.2 Wind turbine nacelle instrumentation

The measurement point with most instrumentation is in the nacelle of wind turbine #1. Here 3 phase voltages and currents are measured together with the shaft torque (low speed) and the high and low rotor speeds.

For safety reasons, the 960 V voltages are measured through the voltage transformers of the control system. However, since the secondary voltage of these transformers exceed $\pm 5V$, three Tektronix P5200 High Voltage Differential Probes are used to measure on the secondary side of the voltage transformers. The 3 dB bandwidth of the Tektronix P5200 probes is from DC to 25 MHz, so the bandwidth is of the combined measurement is probably limited by the voltage transformers, for which we do not know the bandwidth. However, for the present measurements, the bandwidth is assumed to be sufficient with a filter cut-off frequency of 3 kHz as mentioned in section 5.3.1.

The generator currents are measured directly on the cables from the generator to the 960 kV bus bar. The generator has open delta windings, thus the currents in the delta windings are measured directly, and later converted to line currents. The generator currents are measured with flexible LEM-flex RR 3000-SD/48 AC current probes with a 3 dB bandwidth from 8 Hz to 100 kHz, which is also well above the filter cut-off frequency of 3 kHz mentioned in section 5.3.1.

5.3.3 Wind turbine 10 kV terminals instrumentation

Measurements of voltages and currents have been acquired on the 10 kV terminals of three different wind turbines. For the first experiments, these measurements have been acquired only in wind turbine #1, which is tripped in these experiments. For the islanding experiment, the measurement equipment has been moved to the island consisting of wind turbine #2 and #6.

In all cases, the instrumentation has been the same. We have measured on the secondary sides of the voltage and current transformers in the 10 kV metering point. Since these voltage and current transformers do not provide $\pm 5V$ as needed by the data acquisition system, a Risø voltage-box has been applied to convert the voltage transformer secondary sides to three voltage signals within the $\pm 5V$ range, and three LEM PR30 AC/DC current probes have been applied to convert the current transformer secondary sides to three signals within the $\pm 5V$ range.

The 0.5 dB frequency range of the LEM PR30 current probes is 0 to 100 kHz, i.e. well above the filter cut-off frequency of 3 kHz mentioned in section 5.3.1.

The Risø voltage box is based on LEM LV 25-P hall effect transducers. The bandwidth for these transducers is not specified directly, but the 90 % response time is $40 \mu s$ according to the data sheets, which for a first order system corresponds to a time constant $\tau = 40\mu s / 2.3 = 17 \mu s$. Thus, the 3 dB frequency can

be approximated to $f_{3\text{dB}} \approx 1 / (2\pi \cdot \tau) = 9.4 \text{ kHz}$, i.e. well above the filter cut-off frequency of 3 kHz mentioned in section 5.3.1.

5.3.4 Substation 10 kV wind farm collection line instrumentation

The measurement equipment in the substation is similar to the equipment on the 10 kV wind turbine terminals. Only, here the existing 10 kV voltage transformers and current transformers on the incoming feeder in the substation are applied.

5.4 Trip of one wind turbine at 10 kV terminal

5.4.1 Description of experiment

The scope of this experiment is to isolate wind turbine #1 on one of the wind farm collection cables and trip it with the 10 kV breaker at the wind turbine. Figure 26 shows the connection of the wind farm for the experiment. The activated breaker for this experiment is B_{wt1} . In order to minimise disturbances and avoid loss of production on the privately owned wind turbines #3, #4 and #5, these are connected to the substation through the eastern cable, and the NVE owned wind turbine #2 and wind turbine #6 are stopped to avoid overload on the eastern cable.

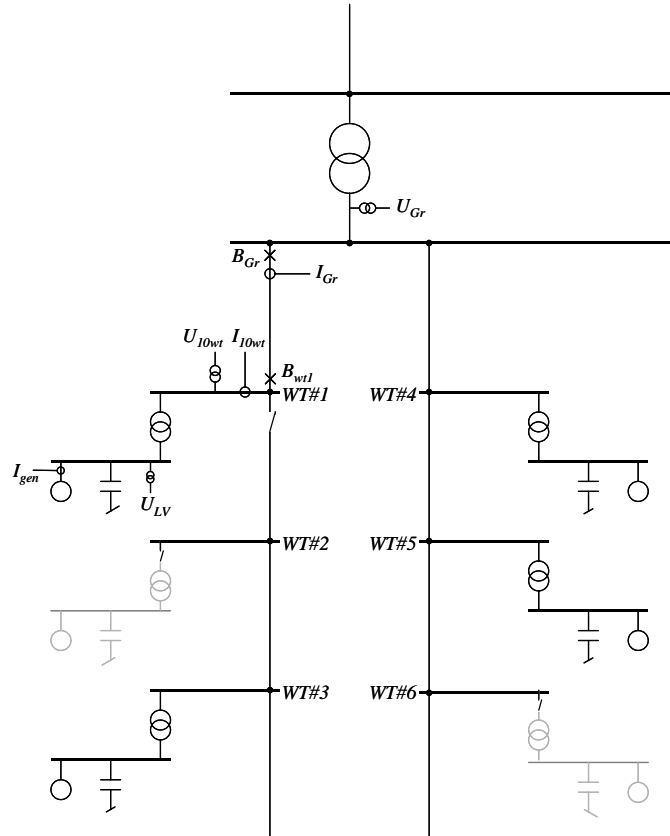


Figure 26. Wind farm connection for trip of wind turbine #1

There are three measurement points. The first measurement point is in the nacelle of wind turbine #1. Here 3 phase voltages U_{LV} and currents I_{gen} are measured together with the mechanical measurements of torque and speed according to the description in chapter 5.3.2.

The second measurement point is on the 10 kV connection point in the tower bottom of wind turbine #1. Here 3 phase voltages U_{10wt} and currents I_{10wt} are measured according to the description in chapter 5.3.3.

The third measurement point is in Grevinge substation. Here 3 phase voltages U_{Gr} and currents I_{Gr} are measured on the western collection cable from the wind farm to the substation according to the description in chapter 5.3.4.

5.4.2 Measurement results

The measurements have been synchronised manually so that the trip of wind turbine #1 is activated at $t=0$. Figure 27 shows the measured line to neutral voltages U_{LV} and Figure 28 show the simultaneous line currents I_{gen} .

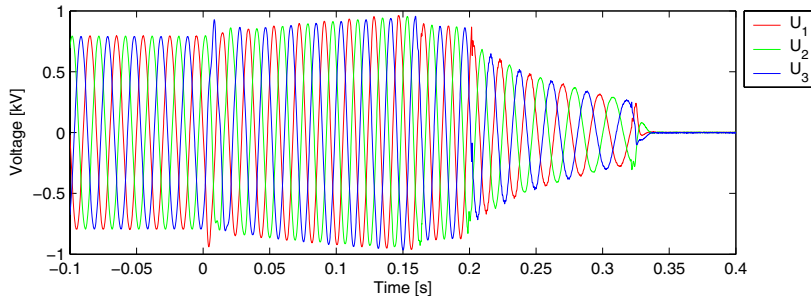


Figure 27: Line to neutral voltages U_{LV} measured at the 960 V bus of the generator of wind turbine #1.

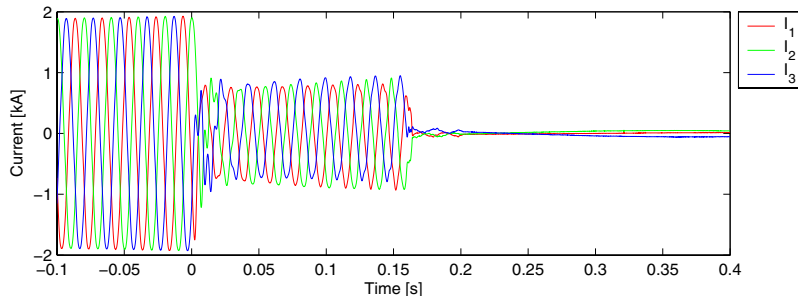


Figure 28: Generator line currents I_{gen} of the generator of wind turbine #1.

It is seen that the voltages increase the first 150 ms and then start to decrease. The currents drop immediately after the trip, and drop to zero after 150 ms. The corresponding instantaneous active and reactive power, calculated according to (9) and (10) respectively are shown in Figure 29.

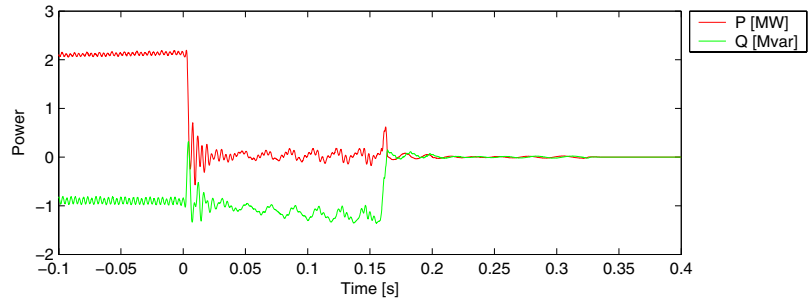


Figure 29: Active and reactive power of the generator of wind turbine #1.

The active power drops immediately after the tripping corresponding to the current drop. This is because the active power cannot be transmitted to the grid any more. Still, the generator is fed with reactive power from the island grid, i.e. from the capacitors. After 150 ms, the generator currents drop to zero because the generator and/or the capacitors are disconnected.

Figure 30 and Figure 31 show the generator speed and the shaft torque in the same period as the electrical time series were shown in the previous figures. It is seen that the shaft torque drops as expected because the electrical torque drops right after the tripping. At the same time, the rotor speed accelerates because the aerodynamic torque is no longer balanced by the shaft torque. The fast speed reaches a maximum, which is mainly due to a combination of two related effects: The first effect is that the blades start to pitch which reduces the aerodynamic torque and soon makes the aerodynamic torque negative which breaks the blade rotor. The second effect is that the shaft spring oscillation changes direction.

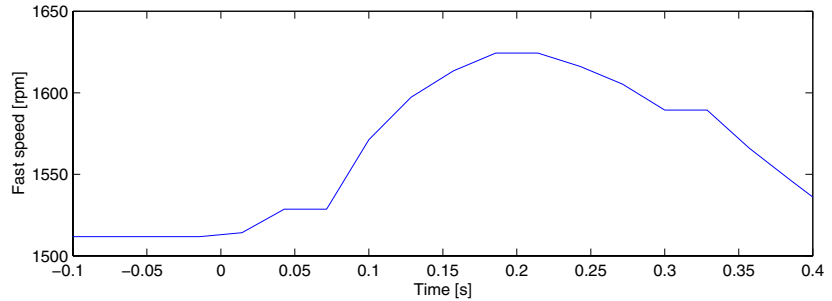


Figure 30: Generator rotor speed of wind turbine #1.

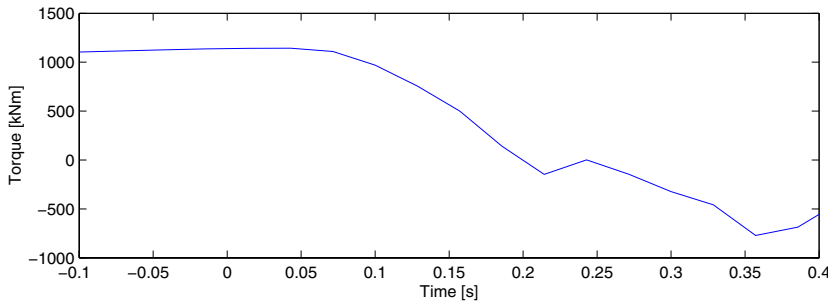


Figure 31: Shaft torque of wind turbine #1.

The oscillation of the drive train is much clearer when we show the speed and torque in a longer time scale as in Figure 32 and Figure 33. As mentioned in section 0, the torque measurement can be used to estimate the stiffness and damping for the drive train model, which has been done, and confirmed good agreement with the first values supplied by NEG-Micon. The next thing which is observed is that there is a significant effect of the backlash in the gearbox, causing the torque to stay around zero for some time when it crosses zero.

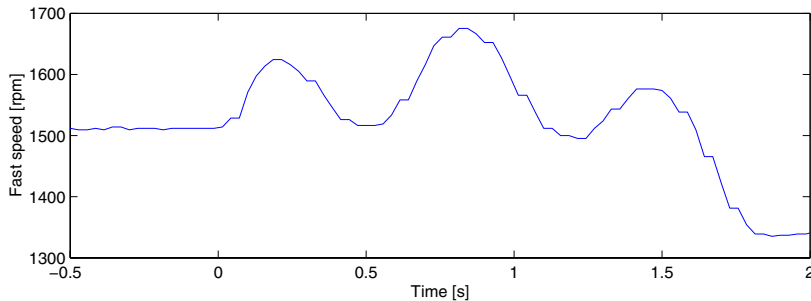


Figure 32: Rotor speed of wind turbine #1.

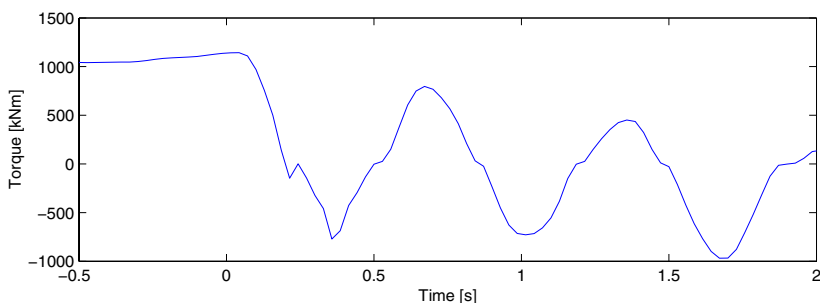


Figure 33: Shaft torque of wind turbine #1.

The frequency of the low voltages in Figure 27 is shown in Figure 34. After the tripping, the slip must come to zero because the power cannot be transmitted to the grid. This makes the frequency increases right after the tripping. Then the frequency follows the generator rotor speed (compare to Figure 30) until the generator trips at 150 ms. After that, the frequency is only changed a little until at 200 ms, where it drops rapidly together with the voltage (Figure 27). The drop in voltage and frequency is a consequence of the trip of the generator and capacitors.

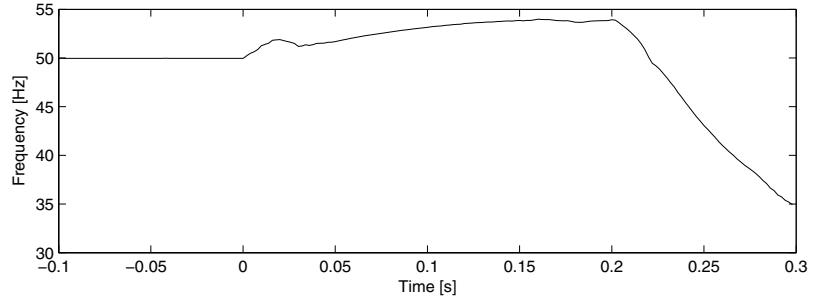


Figure 34: Frequency of low voltage in wind turbine #1.

The measurements of the voltages and currents on the 10 kV wind turbine terminal and the collection cable in Grevinge are shown in Figure 35 -Figure 38.

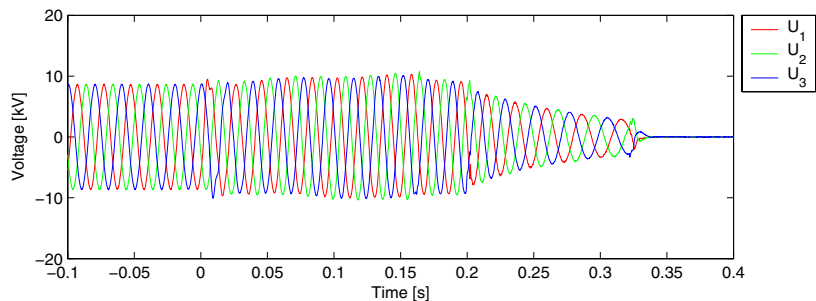


Figure 35: Line to neutral voltages U_{10wt} measured at the 10 kV terminal of wind turbine #1.

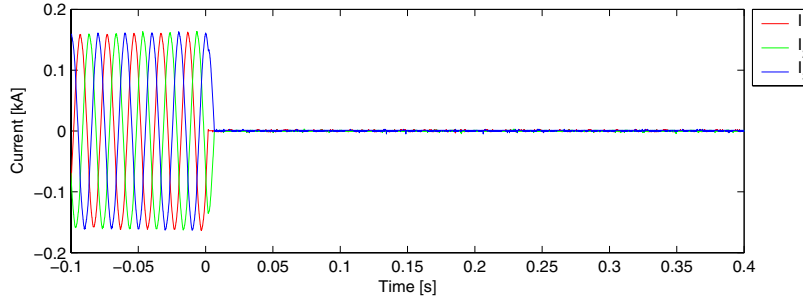


Figure 36: Line currents $I_{10\text{wt}}$ measured at the 10 kV terminal of wind turbine #1.

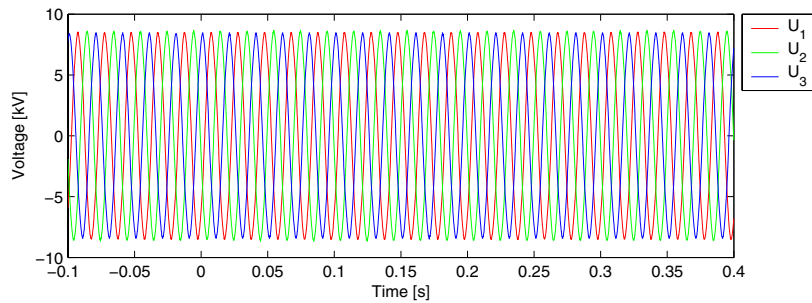


Figure 37: Line to neutral voltages U_{Gr} measured at the western 10 kV wind farm power collection cable in Grevinge substation.

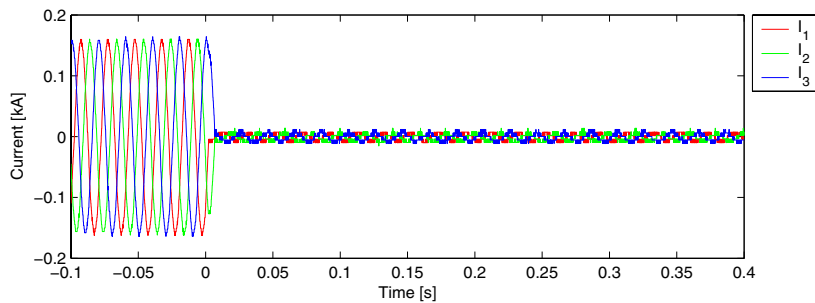


Figure 38: Line currents I_{Gr} measured at the western 10 kV wind farm power collection cable in Grevinge substation.

It is seen that the voltage on the 10 kV terminals of the wind turbine in Figure 35 has a shape very similar to the low voltage bus bar Figure 27, while the distortion of the voltage in Grevinge in Figure 37 is small. It is also seen that the currents at the 10 kV terminals in Figure 36 go to zero immediately, while the current in Grevinge in Figure 38 keeps a small value after the tripping, feeding

capacitive current to the unloaded power collection line. It should be noted that the distinct steps in the currents Figure 38 is due to discretisation noise, because the gain in the SCXI-1141 lowpass filters (see section 5.3.1) was set too small for the current measurements in Grevinge, and consequently these current signals for the ADC are small. However, this is not critical for the present study.

5.5 Trip of 10 kV wind farm collection cable at substation

5.5.1 Description of experiment

The scope of this experiment is to isolate wind turbine #1 on one of the wind farm collection cables as illustrated in Figure 26, and trip the collection cable with the 10 kV breaker in Grevinge substation B_{Gr} . The measurement points are the same as in the previous experiment, i.e. U_{LV} and I_{gen} together with the mechanical loads in the nacelle of wind turbine #1, U_{10wt} and I_{10wt} at the 10 kV connection point of wind turbine #1, and U_{Gr} and I_{Gr} on the collection cable in Grevinge substation.

5.5.2 Measurement results

The measurements have been synchronised manually so that the trip of the collection cable is activated at $t=0$. Figure 39 shows the line to neutral voltages U_{LV} and the simultaneous generator line currents I_{gen} are shown in Figure 40.

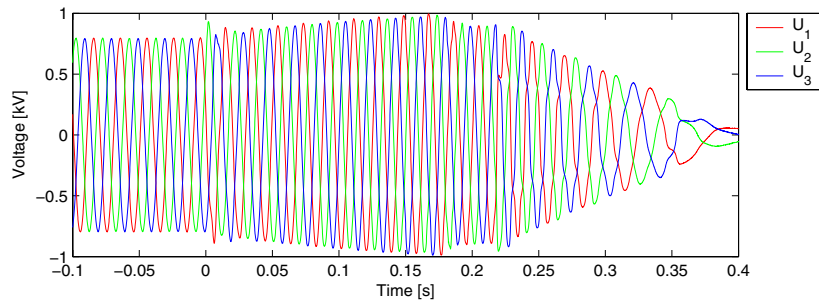


Figure 39: Line to neutral voltages U_{LV} measured at the 960 V bus bar of wind turbine #1.

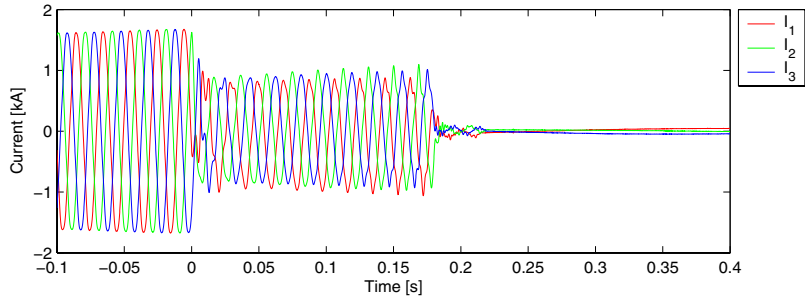


Figure 40: Measured line currents I_{gen} of the generator of wind turbine #1.

It is seen that the voltages increase the first 180 ms and then start to decrease. The current drops immediately after the trip because the power cannot be exported to the grid any more, and goes to zero after 180 ms because generator and/or capacitor is disconnected.

Figure 41 and Figure 42 show the rotor speed and the shaft torque. The oscillation of the drive train is quite similar to the oscillations measured in the previous experiment, shown in Figure 32 and Figure 33.

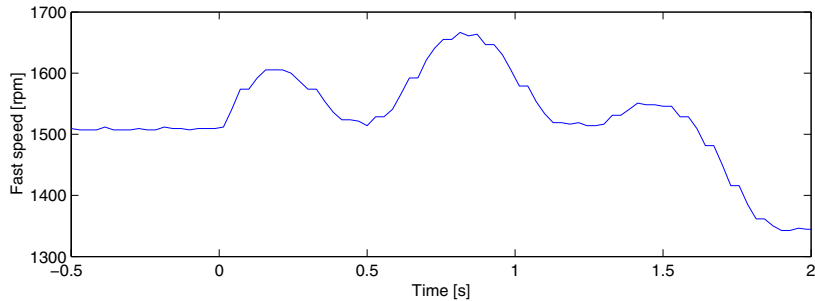


Figure 41: Rotor speed of wind turbine #1.

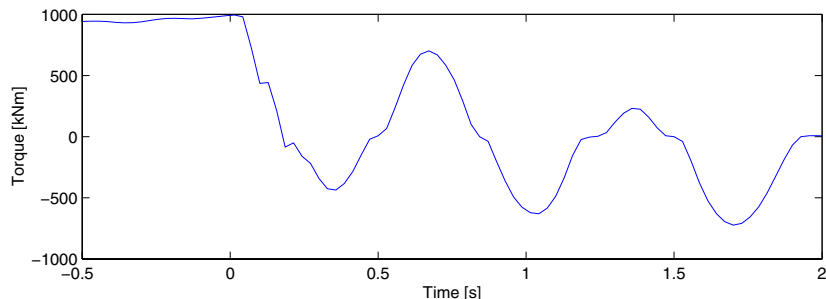


Figure 42: Shaft torque of wind turbine #1.

The measurements of the voltages and currents on the 10 kV wind turbine terminal and the collection cable in Grevinge substation are shown in Figure 43 - Figure 46.

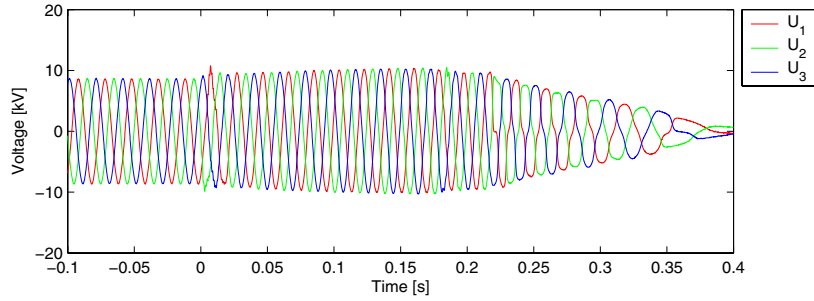


Figure 43:Line to neutral voltages U_{10wt} measured at the 10 kV connection point of wind turbine #1.

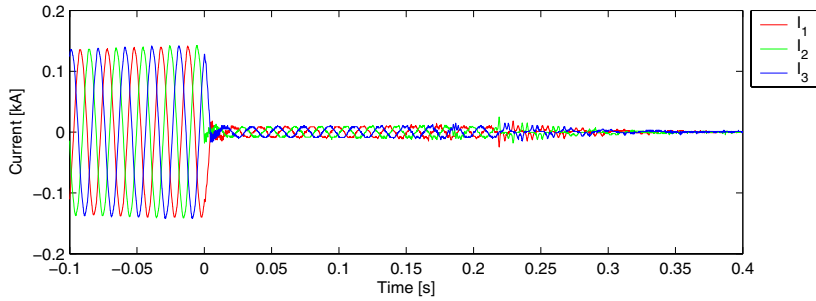


Figure 44:Line currents I_{10wt} measured at the 10 kV connection point of wind turbine #1.

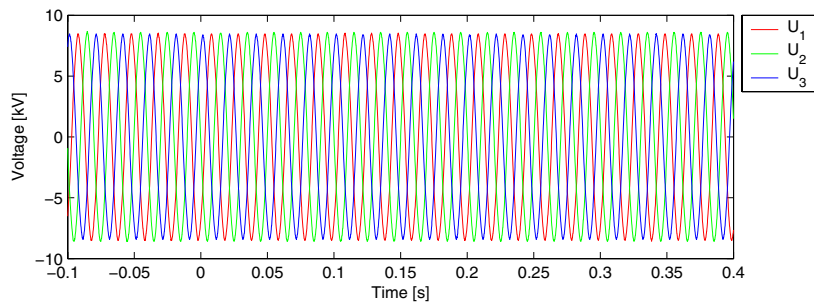


Figure 45:Line to neutral voltages U_{Gr} measured at the western 10 kV wind farm power collection cable in Grevinge substation.

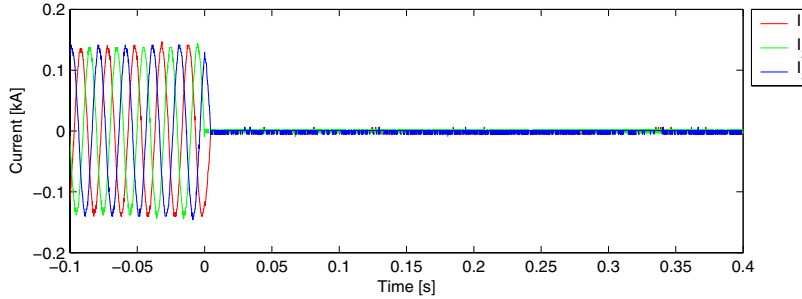


Figure 46: Line currents I_{Gr} measured at the western 10 kV wind farm power collection cable in Grevinge substation.

It is seen that the voltage on the 10 kV terminals of the wind turbine has a shape very similar to the generator voltage, while the distortion of the voltage in Grevinge is small. It is also seen that the currents at the 10 kV terminals keep a small value after the tripping, because in this experiment the capacitive current to the power collection line is fed from the wind turbine, and that these currents decrease with the voltage. The currents in Grevinge go to zero immediately because there is no load seen from Grevinge in this case.

5.6 Emergency stop of one wind turbine

5.6.1 Description of experiment

The scope of this experiment is to isolate wind turbine #1 on one of the wind farm collection cables as illustrated in Figure 26, and activate the emergency stop of wind turbine #1. The measurement points are the same as in the previous experiments, i.e. U_{LV} and I_{gen} together with the mechanical loads in the nacelle of wind turbine #1, U_{10wt} and I_{10wt} at the 10 kV connection point of wind turbine #1, and U_{Gr} and I_{Gr} on the collection cable in Grevinge substation.

5.6.2 Measurement results

The measurements have been synchronised manually so that the emergency stop of wind turbine #1 is activated at $t=0$. Figure 47 shows the line to neutral voltages U_{LV} and the simultaneous line currents I_{gen} are shown in Figure 48.

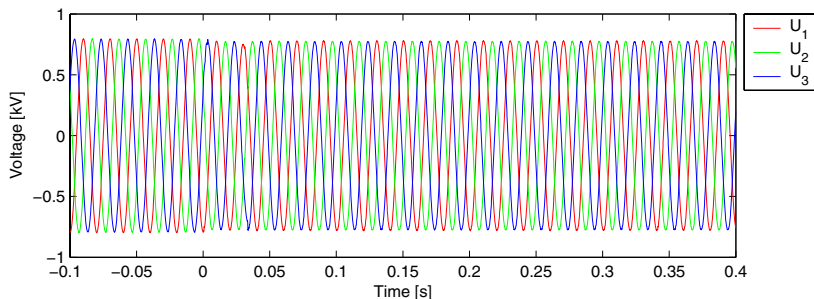


Figure 47: Line to neutral voltages U_{LV} measured at the 960 V bus bar of wind turbine #1.

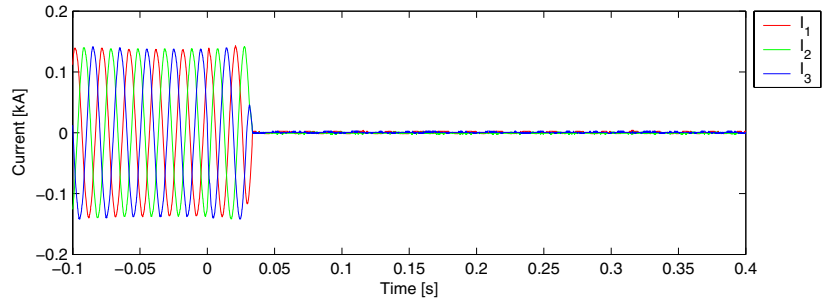


Figure 48: Measured line currents I_{gen} of the generator of wind turbine #1.

It is seen that the effect on the voltage U_{LV} is small, because the wind turbine stays on the grid. However, the generator is disconnected, and the currents drop immediately after the activation of the emergency stop, and goes to zero already after approximately 1.5 line periods. The corresponding instantaneous active and reactive power, calculated according to (9) and (10) respectively are shown in Figure 49. It shows that the active power and the corresponding reactive power decreases at time $t=0$, which could be due to blade pitching and/or mechanical braking.

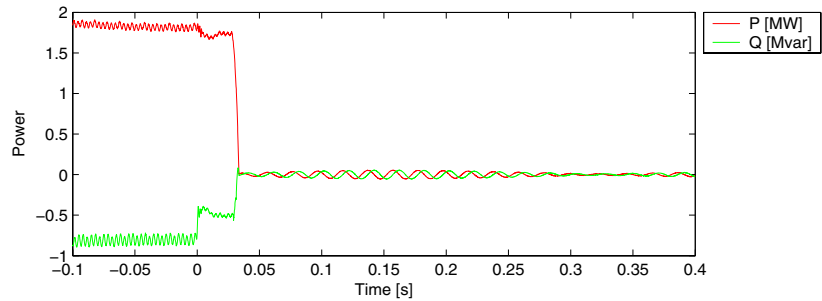


Figure 49: Active and reactive power of the generator of wind turbine #1.

Figure 50 and Figure 51 show the oscillations in the generator speed and the shaft torque after activation of the emergency stop. The torque in this case oscillates around a mean value greater than zero, probably because the mechanical brakes are active during the emergency stop. As a consequence, there is no backlash in the torque, and it is also seen that the period time for the torque oscillations is reduced with approximately 15 % compared to Figure 33, which is likely to be due to the missing backlash. Thus, if backlash is introduced in a future model, the estimation of the stiffness would be more complex.

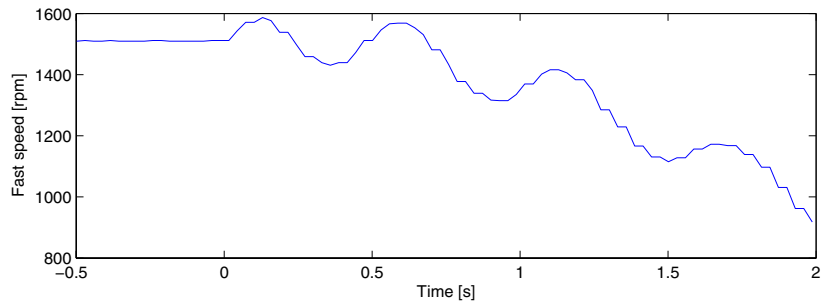


Figure 50: Generator speed of wind turbine #1.

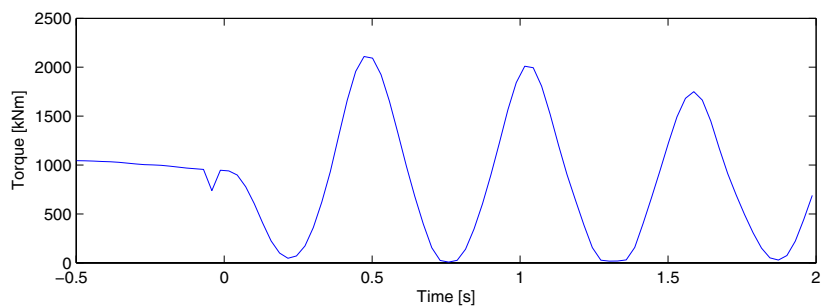


Figure 51: Shaft torque of wind turbine #1.

The measurements of the voltages, currents and power on the 10 kV wind turbine #1 connection point and the collection cable in Grevinge are shown in Figure 52 - Figure 57.

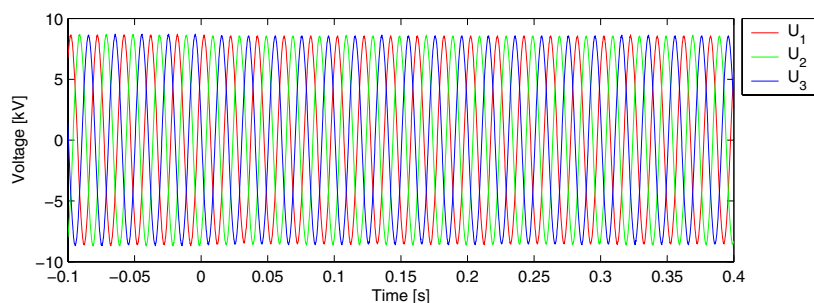


Figure 52: Line to neutral voltages $U_{10\text{wt}}$ measured at the 10 kV connection point of wind turbine #1.

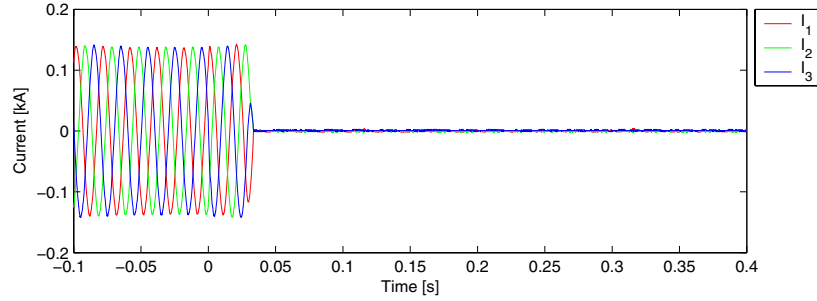


Figure 53: Line currents $I_{10\text{wt}}$ measured at the 10 kV connection point of wind turbine #1.

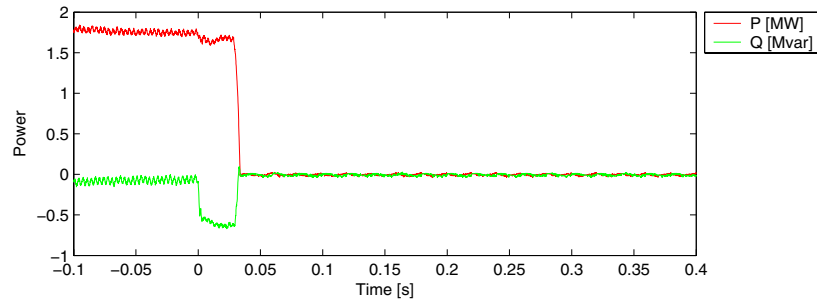


Figure 54: Active power $P_{10\text{wt}}$ and reactive power $Q_{10\text{wt}}$ measured at the 10 kV connection point of wind turbine #1.

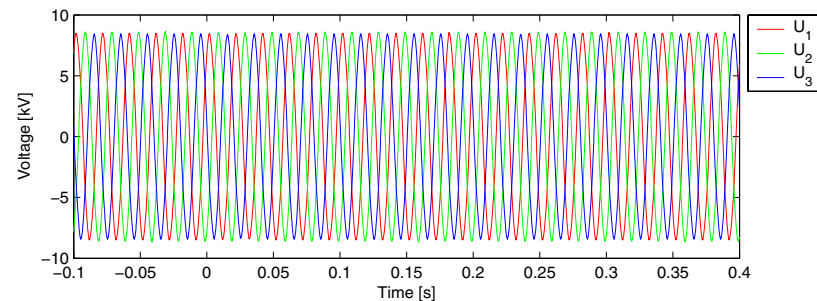


Figure 55: Line to neutral voltages U_{Gr} measured at the western 10 kV wind farm power collection cable in Grevinge substation.

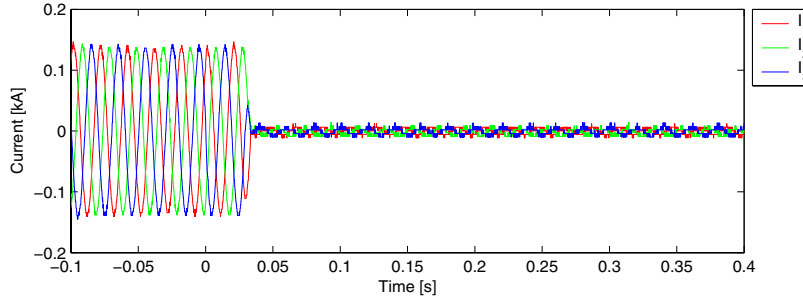


Figure 56: Line currents I_{Gr} measured at the western 10 kV wind farm power collection cable in Grevinge substation.

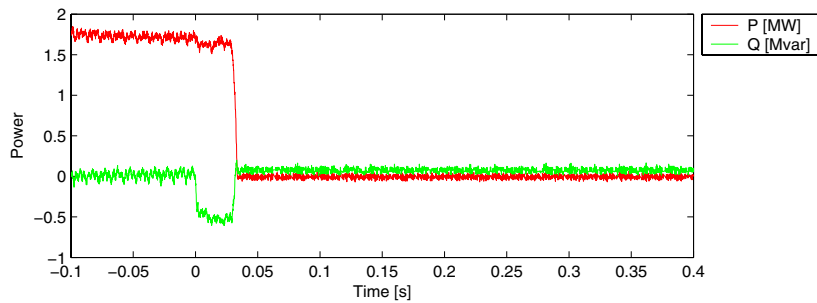


Figure 57: Active power P_{Gr} reactive power Q_{Gr} measured at the western 10 kV wind farm power collection cable in Grevinge substation.

It is seen that the distortion of the voltages is small. It is also seen that the currents at the 10 kV terminals go to zero immediately, while the current in Grevinge keeps a small value after the tripping, feeding capacitive current to the power collection line. Finally, note that $t = 0$ has been selected as the first time where something transient happens, and that the first thing which happens according to reactive power in Figure 54 and Figure 57 is that the capacitors are tripped which causes the wind turbine to consume reactive power (i.e. reactive power becomes negative), and very short after that (at approximately $t = 30$ ms), also the generator is tripped. After both capacitors and generator are tripped, constant reactive power is produced from the cable to the substation as seen in Figure 57.

5.7 Islanding of two wind turbines

5.7.1 Description of experiment

The scope of this experiment is to isolate wind turbine #1, #2 and #6 on one of the wind farm collection cables and trip wind turbine #2 and #6 with the 10 kV breaker at wind turbine #1 on the cable to wind turbine #2. Figure 58 shows the connection of the wind farm for the experiment. The activated breaker for this

experiment is B_{wt12} . In order to avoid overload of the western collection cable and not to take any risks with the privately owned wind turbines, the privately owned wind turbine #3 is stopped during the experiment.

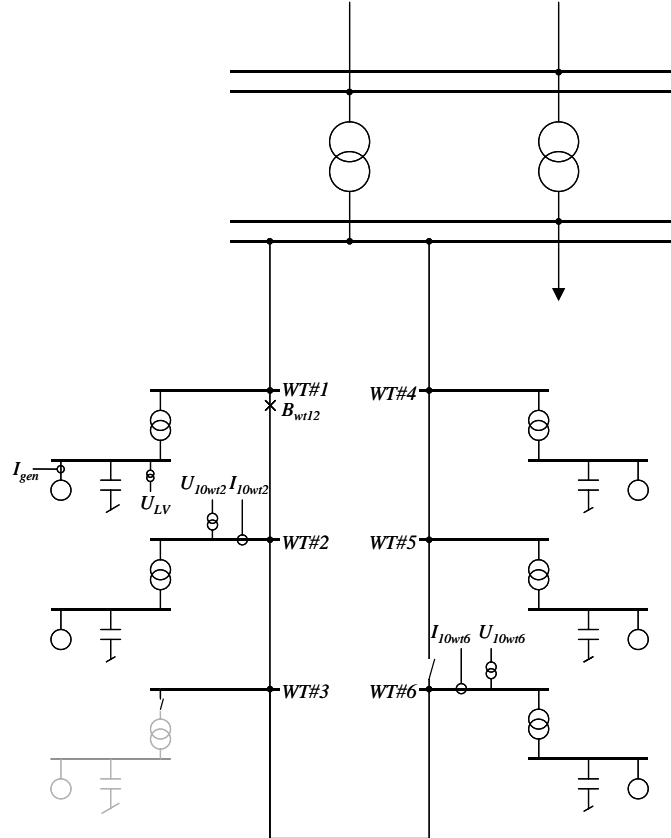


Figure 58. Wind farm connection for trip of wind turbine #2 and #6.

There are two measurement points on the island. The first measurement point is on the 10 kV connection point in the tower bottom of wind turbine #2. Here 3 phase voltages U_{10wt2} and currents I_{10wt2} are measured according to the description in chapter 5.3.3.

The second measurement point is on the 10 kV connection point in the tower bottom of wind turbine #6. Here 3 phase voltages U_{10wt6} and currents I_{10wt6} are measured according to the description in chapter 5.3.3.

Also a measurement point in the nacelle of wind turbine #1 was prepared. However the measurements in the nacelle failed during this experiment.

5.7.2 Measurement results

The measurements of the voltages, currents and power on the 10 kV wind turbines #2 and #6 connection points are shown in Figure 59 - Figure 64, and the frequency of the voltage is shown in Figure 65.

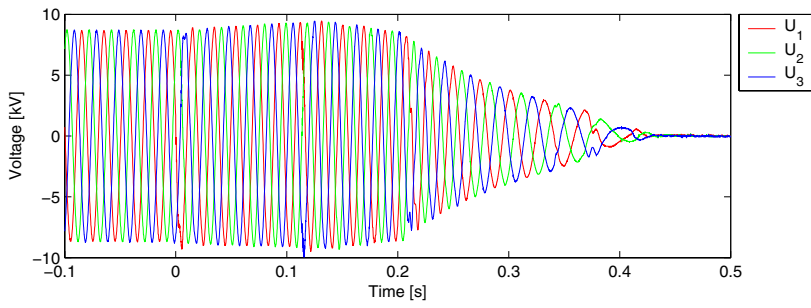


Figure 59: Line to neutral voltages $U_{10\text{wt}2}$ measured at the 10 kV connection point of wind turbine #2.

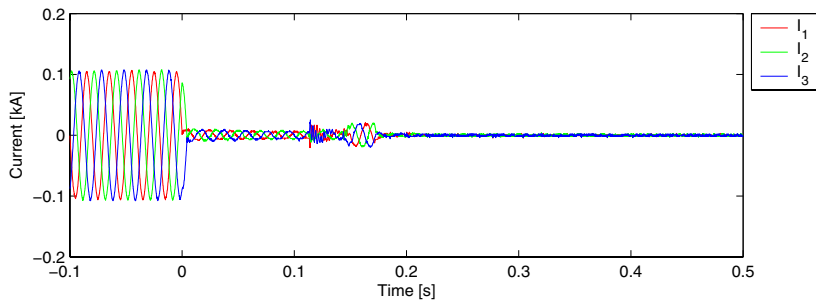


Figure 60: currents $I_{10\text{wt}2}$ measured at the 10 kV connection point of wind turbine #2.

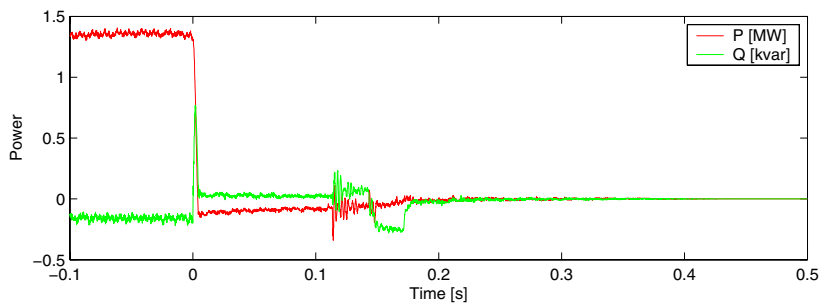


Figure 61: Active power $P_{10\text{wt}2}$ and reactive power $Q_{10\text{wt}2}$ measured at the 10 kV connection point of wind turbine #2.

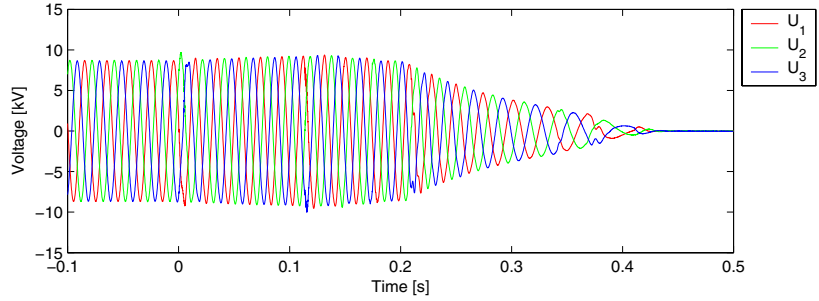


Figure 62: Line to neutral voltages $U_{10\text{wt6}}$ measured at the 10 kV connection point of wind turbine #6.

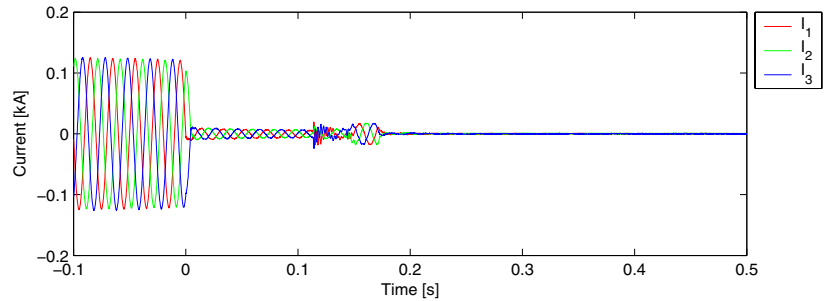


Figure 63: Line currents $I_{10\text{wt6}}$ measured at the 10 kV connection point of wind turbine #6.

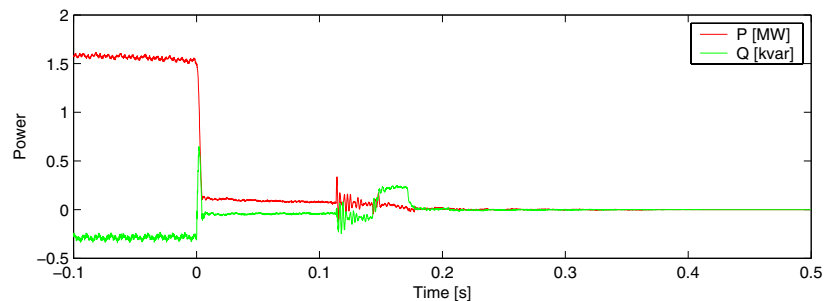


Figure 64: Active power $P_{10\text{wt6}}$ and reactive power $Q_{10\text{wt6}}$ measured at the 10 kV connection point of wind turbine #6.

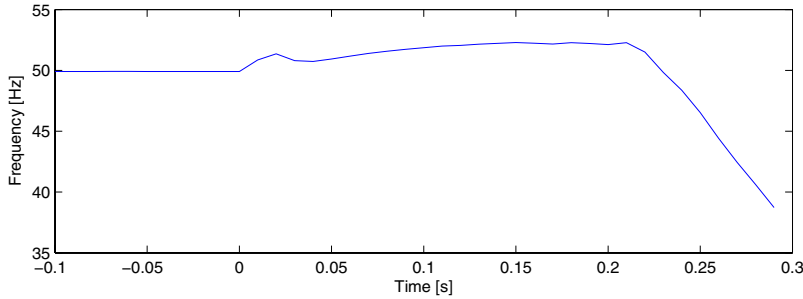


Figure 65: Frequency of the voltage U_{10wt2} measured at the 10 kV connection point of wind turbine #2.

Initially, the wind turbines do not produce the same power and they also consume different amount of reactive power. Wind turbine #6 produces more than wind turbine #2, apparently because the wind speed is a little higher at wind turbine #6 when the island is established by the tripping. As a consequence, wind turbine #6 will rotate slightly faster than wind turbine #2. When the wind turbines are isolated, power cannot flow into the grid any more, and a new “steady state” with a higher grid frequency must occur (confirmed in Figure 65), so that the average of the slips in the two wind turbines becomes zero. Since wind turbine #6 rotates faster, it will get a positive slip in the new steady state, while wind turbine #2 will get a corresponding negative slip, and consequently power will flow from #6 to #2, which is also seen to be the case from $t = 0$ to $t=0.11$ s.

5.8 Voltage change due to tripping

5.8.1 Description of experiment

The scope of this experiment is to isolate wind turbine #1, #2 and #6 on one of the wind farm collection cables and trip wind turbine #2 and #6 with the 10 kV breaker at wind turbine #1 on the cable to wind turbine #2 as described in section 5.7.1.

In the present experiment, there are two measurement points. The first measurement point is in the nacelle of wind turbine #1. Here 3 phase voltages U_{LV} and currents I_{gen} are measured together with the mechanical measurements of torque and speed according to the description in chapter 5.3.2.

The second measurement point is on the 10 kV connection point in the tower bottom of wind turbine #6. Here 3 phase voltages U_{10wt6} and currents I_{10wt6} are measured according to the description in chapter 5.3.3.

5.8.2 Measurement results

The measurements of the voltages, currents and instantaneous power on the low voltage side of wind turbine #1 are shown in Figure 66 and Figure 68. The tripping is seen clearly on the currents and on the power, but it is not immediately visible on the voltage. However, the changes in currents and power are due to a voltage change, because wind turbine #1 can only see the tripping of the two neighbouring wind turbines because it changes the voltage. Note that Figure 68 shows very clearly the 50 Hz fluctuations, which are due to the generator stator flux transients.

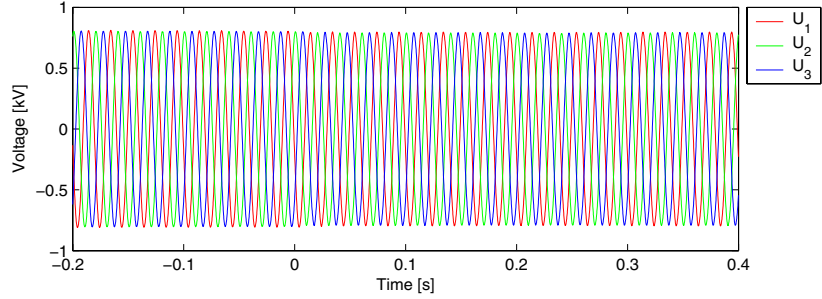


Figure 66: Line to neutral voltages U_{LV} measured at the 960 V bus of wind turbine #1.

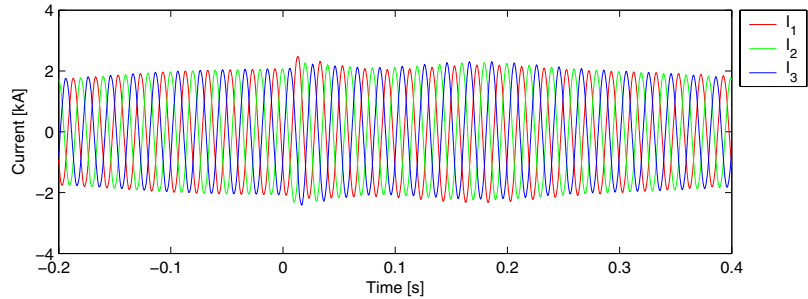


Figure 67: Measured line currents I_{gen} of the generator of wind turbine #1.

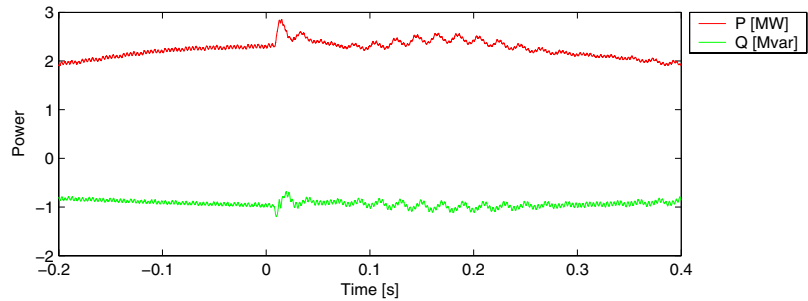


Figure 68: Active power P_{gen} and reactive power Q_{gen} of the generator of wind turbine #1.

The change in voltage is much clearer from the positive sequence of the voltage shown in Figure 69. The reason why the voltage step down ramp seems to last 20 ms is that the software uses a full line period to fit the fundamental, and therefore the full effect is not seen before the voltage has decreased in a full line period.

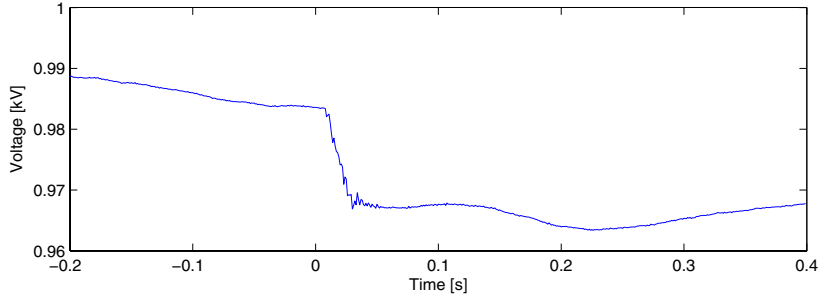


Figure 69: Positive sequence of the low voltage U_{LV} of wind turbine #1.

Figure 70 shows the power from the 10 kV terminal of wind turbine #6. When the wind turbines #2 and #6 were tripped, #6 produced 1.9 MW and consumed 250 kvar reactive power. Unfortunately, the power is not available from wind turbine #2, but we will assume that it has been in the same state, although it probably produced a little less, since wind turbine #6 produces power in the island (after $t = 0$), and this power must be consumed by turbine #2 as it was the case in the previous islanding experiment (see Figure 61 and Figure 64).

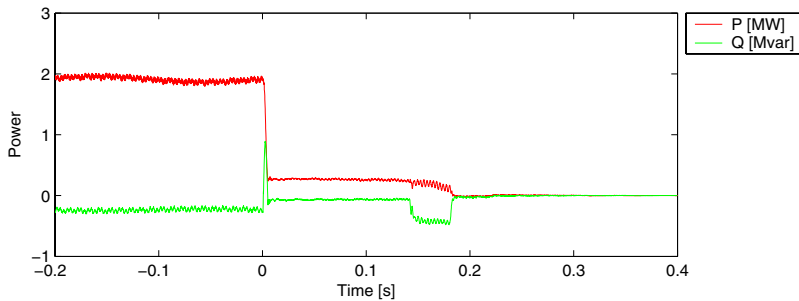


Figure 70: Active and reactive power from wind turbine #6.

5.9 Voltage change due to tap position changing

5.9.1 Description of experiment

The scope of this experiment is manually and online to change the tap position of the substation transformer Tr#1, to which the whole wind farm is connected as indicated in Figure 6.

In the present experiment, there are two measurement points. The first measurement point is in the nacelle of wind turbine #1. Here 3 phase voltages U_{LV} and currents I_{gen} are measured together with the mechanical measurements of torque and speed according to the description in chapter 5.3.2.

The second measurement point is on the 10 kV connection point in the tower bottom of wind turbine #6. Here 3 phase voltages U_{10wt6} and currents I_{10wt6} are measured according to the description in chapter 5.3.3.

5.9.2 Measurement results

The measurements of the voltages, currents and instantaneous power on the low voltage side of wind turbine #1 are shown in Figure 71 - Figure 73. The change of tap position is not immediately visible on the voltages, but it is seen clearly on the power as excitation of stator flux transients with fundamental frequency (50 Hz). However, the changes in power is due to a voltage change, because wind turbine #1 can only see the tap change because it changes the voltage.

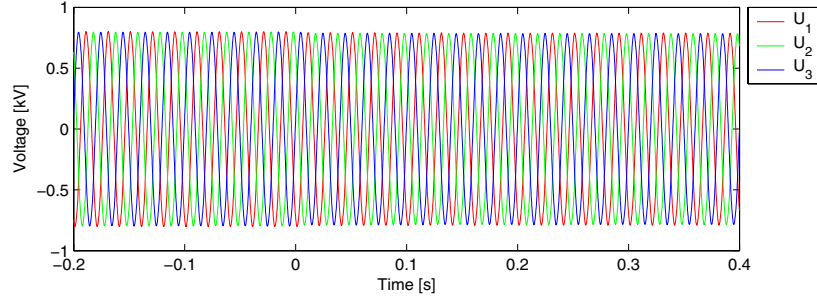


Figure 71: Line to neutral voltages U_{LV} measured at the 960 V bus of wind turbine #1.

Figure 72 indicates that the currents drop the first line period after the tap change. The other, much slower fluctuations in the currents are due to turbulence in the wind speed, which is also seen as slow power variations in Figure 73.

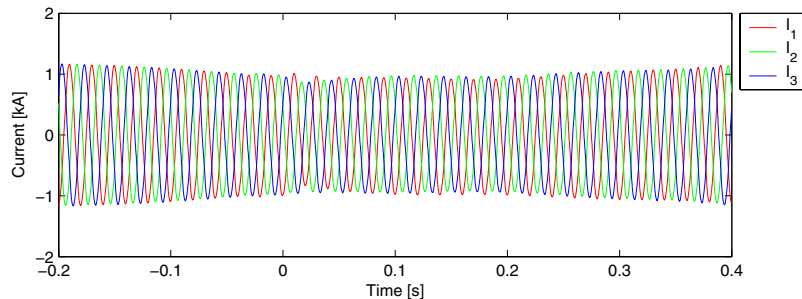


Figure 72: Measured line currents I_{gen} of the generator of wind turbine #1.

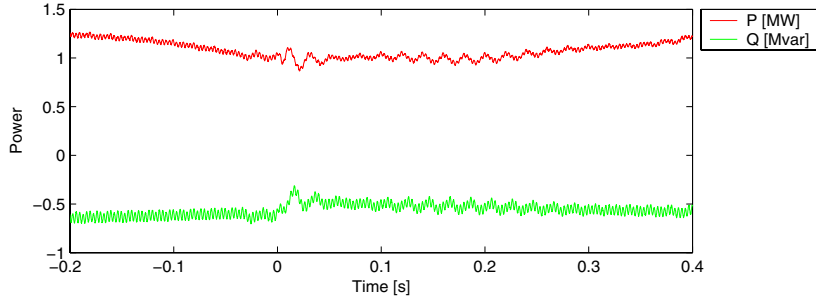


Figure 73: Active power P_{gen} and reactive power Q_{gen} of the generator of wind turbine #1.

The change in voltage is much clearer from the positive sequence of the voltage shown in Figure 74. There is a distinct increase in voltage before it decreases, which has been confirmed to be general by several repetitions of the experiment. The voltage shape in Figure 74 indicates that the tap change is not a simple switch from one position to another of the tap position, but the coupling is somehow softened.

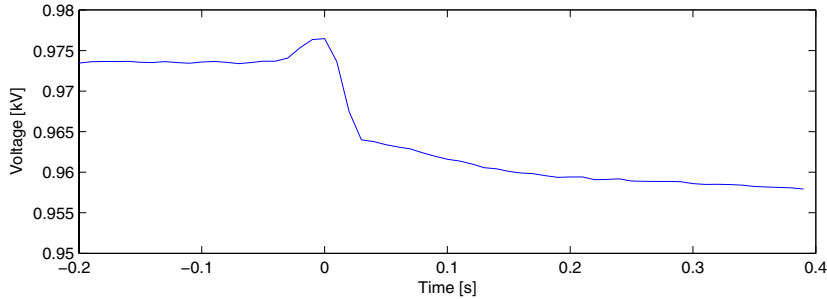


Figure 74: Positive sequence of the low voltage U_{LV} of wind turbine #1.

6 Comparison of simulations and measurements

6.1 General

In this chapter, results from simulations of the transient events described in chapter 5 are presented and compared to the measurements. The simulations are done either with the DIgSILENT model or with the EMTDC model.

6.2 Trip of one wind turbine at 10 kV terminal

The experiment “Trip of one wind turbine at 10 kV terminal” is described in section 5.4. This experiment has been simulated with the DIgSILENT model. In the present section, we will present the simulation results and compare them to the measurements.

Figure 75 shows the simulated line to neutral voltages U_{LV} at the 960 V bus of wind turbine #1. Compared to the corresponding measured voltages in Figure 27, it is immediately seen that the voltages increase in the first 150 ms in simulations as well as measurements. At that time, the contactors on generator and capacitors are activated to open. However, each contactor will not open before the first zero crossing of the corresponding current. After 200 ms the measured voltages seem to decrease almost exponentially and the frequency in Figure 34 decreases fast but continuously. At the same time (after 200 ms), the simulated voltage drops immediately to zero. The difference is probably due to the hydraulic pump, which is not included in the simulations. That small electrical machine would prevent the voltage from dropping to zero immediately after generator and capacitors are disconnected, even though its inertia is very small. Thus, the measured and simulated voltages increase quite similarly in the first 150 ms, but after that they come to zero quite differently, probably because a hydraulic pump is active, and this is not included in the simulations.

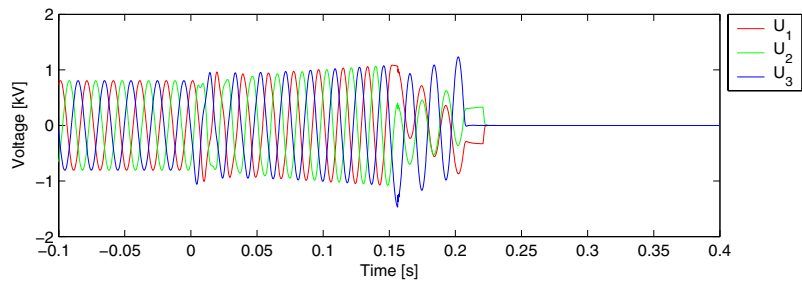


Figure 75: Simulated line to neutral voltages U_{LV} at the 960 V bus of wind turbine #1.

Figure 76 shows the simulated line currents I_{gen} of the generator of wind turbine #1. Compared to the corresponding measured currents in Figure 28, it is immediately seen that the currents increase in the first 150 ms in simulations as well as measurements. After that, both measured and simulated currents drop to zero because the generator is disconnected. Thus, simulated and measured generator currents immediately look very similar in the whole time interval.

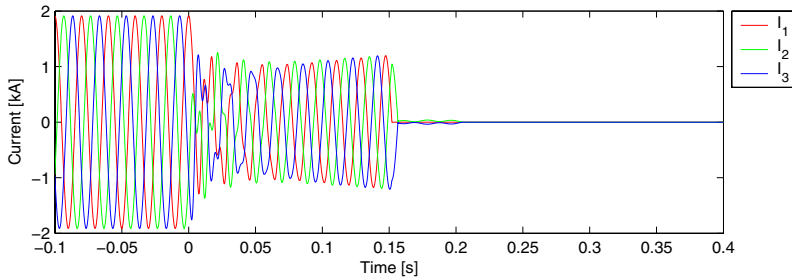


Figure 76: Simulated line currents I_{gen} of the generator of wind turbine #1.

Figure 77 compares measured and simulated (DIgSILENT) instantaneous generator power of wind turbine #1. Simulation and measurement agree very well the first 5 ms after the tripping, where the power drops to zero. After that, the simulations show significant oscillations with approximately 220 Hz, which can be seen also in the measurements, but much less significant, and at a higher frequency. Moreover, the measured power shows 50 Hz oscillations in the power, which are not present in the simulations.

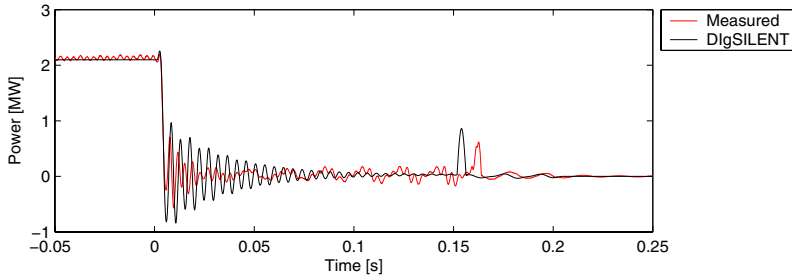


Figure 77: Measured and simulated (DIgSILENT) generator power of wind turbine #1.

An attempt has been done to identify the 220 Hz oscillations in the simulations. From the equivalent in Figure 16, when the wind turbine is tripped on the 10 kV terminals, the capacitor $C=C_{WTI}$ approximately looks into the inductance $L=L_{Gs}+L_{Gr}$. Seen from C_{WTI} , the other capacitors can be discarded because they are decays lower than C_{WTI} , and the shunt inductances L_{T2m} and L_{Gm} can be discarded because they are decays higher than the serial inductances. Inserting these values for C and L in ((6)), an eigenfrequency $f=156$ Hz is found. Thus, this estimate provides an order of magnitude of the frequency, but not an exact value. However, to simplify the estimation, the generator model has been approximated to $L=L_{Gs}+L_{Gr}$, where L_{Gs} represents X_s and L_{Gr} represents X_{r0} in Figure 9. A more detailed eigenfrequency study has not been performed.

An attempt has been done to improve the simulation by including iron losses in the generator model, which will in principle damp the oscillation between C_{WTI} and the inductances. However, that only changed the simulation result marginally, because the iron losses are very small, and consequently the damping effect is very small.

Another reason for the difference in the 220 Hz component could be saturation effects. However, this has not been investigated further.

The other difference is the 50 Hz oscillations in the measured power after the tripping. The amplitude of this oscillation is almost 100 kW, and it originates from dc components in the measured line currents after the tripping.

Figure 78 compares measured and simulated instantaneous reactive power from the generator of wind turbine #1. Like for the active power, simulation and measurement agree very well the first 5 ms after the tripping, where the reactive power has a significant spike of approximately 1.5 Mvar. After that, the simulations show significant oscillations with approximately 220 Hz, which can be seen also in the measurements, but in the measurements these oscillations are damped much faster.

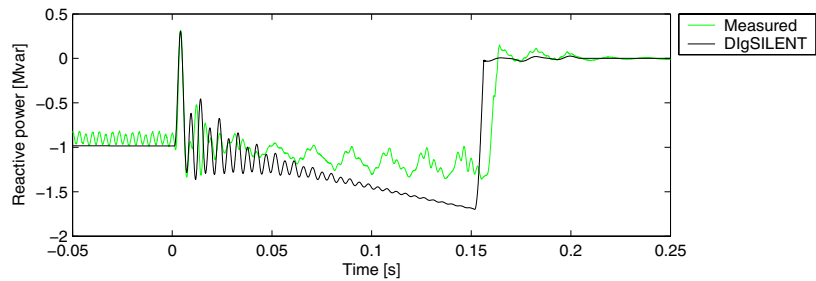


Figure 78: Measured and simulated (DIgSILENT) generator reactive power of wind turbine #1.

Yet, the most important difference between simulation and measurement of reactive power in Figure 78 is the fast increase in reactive power consumption after the tripping, which is observed in the simulations. This is related to the voltage increases, which is much faster in the simulations than in the measurements as shown in Figure 79. This faster increase in the simulated voltage could be because of the uncertainty in the generator parameters mentioned in section 3.3.1, and the omission of saturation in the models is also a possible explanation. Figure 79 shows that the voltage increases quite linearly in the simulations after $t=0.05$ s, while the measured voltage has a more non-linear behaviour. This difference confirms that saturation can be the main explanation, because saturation introduces a non-linearity.

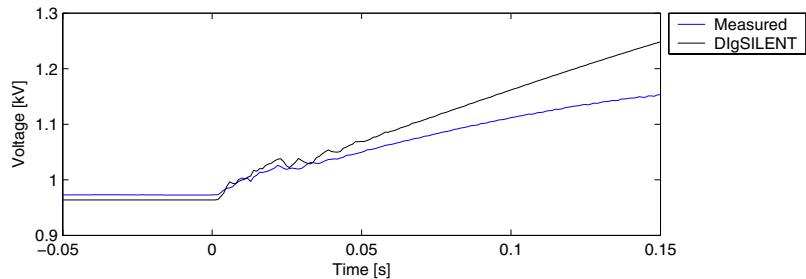


Figure 79: Measured and simulated (DIgSILENT) positive sequence of generator voltage in wind turbine #1.

Figure 80 shows measured and simulated generator speed of wind turbine #1. Here, there is a very good agreement in the first second, but after that, the simulated speed decreases slower than the measured. The main explanation for that is probably that dynamic inflow is not included in the aerodynamic model as mentioned in 3.3.3. Dynamic inflow generally enforces the immediate effect of pitching the blades, until the inflow reaches a new steady state, and thus the dynamic inflow effectively increases the effect of the pitching until the new steady state is reached.

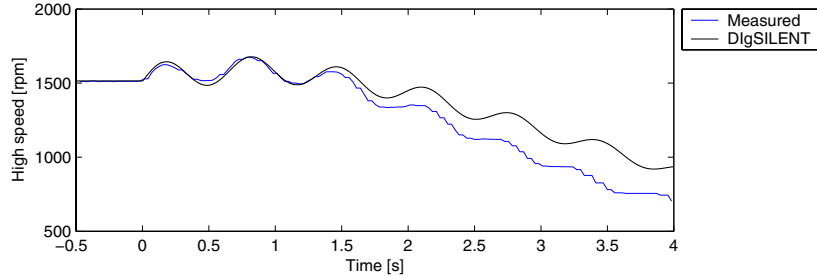


Figure 80: Measured and simulated (DiGILENT) generator speed of wind turbine #1.

Figure 81 shows the corresponding measured and simulated shaft torques. The comparison confirms that backlash is relevant to include in the models, because backlash not only causes small simulation errors in the zero crossings, but also, as a consequence of the error in the zero crossings, the frequency of the oscillation is changed.

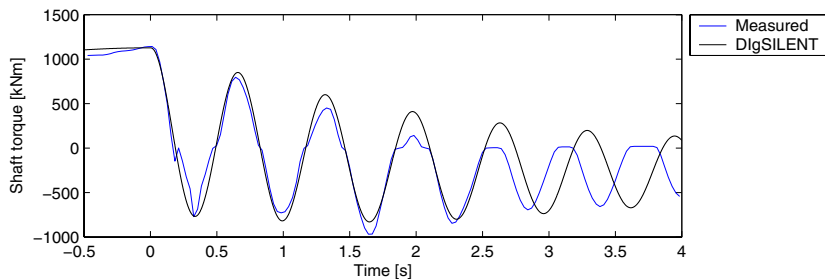


Figure 81: Measured and simulated (DiGILENT) shaft torque of wind turbine #1.

Figure 82 compares measured and simulated voltages at the 10 kV terminal of wind turbine #1. This voltage is very similar in shape to the low voltages in Figure 79, because the transformer connects these two voltages during the whole experiment.

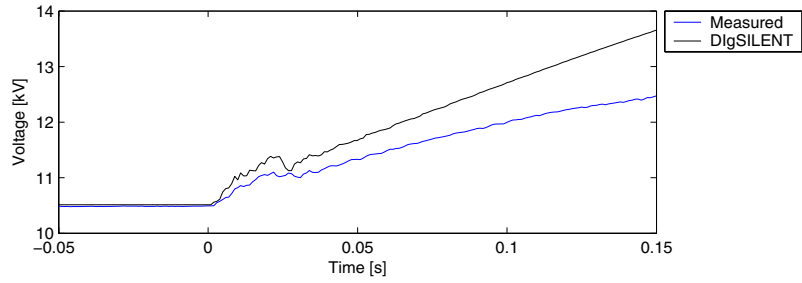


Figure 82: Measured and simulated (DIgSILENT) voltage at 10 kV terminal of wind turbine #1.

Figure 83 compares measured and simulated reactive power at the 10 kV terminals of wind turbine #1. This comparison is very convincing as a validation of the simulation. Comparing to the reactive power at the low voltage terminals in Figure 78, it is seen that the spike in the first few milliseconds after the tripping is transmitted from the tripped wind turbine to the grid even though the breaker has been opened. This is because an arc conducts the current until the first zero crossing. After the arc is cleared, the transmitted reactive power becomes zero.

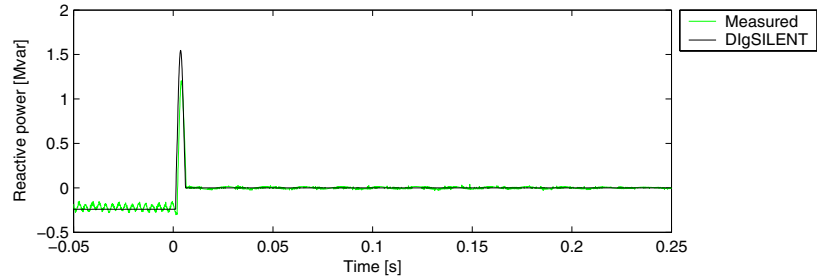


Figure 83: Measured and simulated (DIgSILENT) reactive power at 10 kV terminal of wind turbine #1.

Figure 84 compares the frequency of the measured voltage U_{LV} on the low voltage terminals. The frequency of the voltage on the 10 kV terminal is quite similar as expected, so this frequency will not be shown here. It is seen that the frequency of the simulated frequency increases faster than the measured, which corresponds to that the simulated generator speed in Figure 80 also increases faster than the measured in the first 150 ms after the tripping.

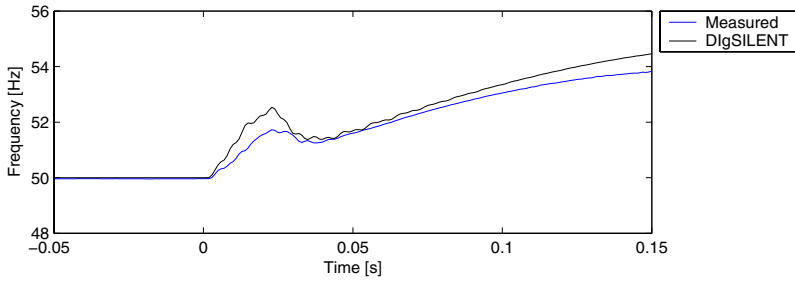


Figure 84: Measured and simulated (DiGILENT) frequency of U_{LV} of wind turbine #1.

6.3 Trip of 10 kV wind farm collection cable at substation

The experiment “Trip of 10 kV wind farm collection cable at substation” is described in section 5.5. This experiment has been simulated with the DiGILENT model. In the present section, we will present the simulation results and compare them to the measurements.

Figure 85 shows the simulated line to neutral voltages U_{LV} at the 960 V bus of wind turbine #1. Compared to the corresponding measured voltages in Figure 39, it is immediately seen that the voltages increase in the first 150 ms in simulations as well as measurements. However, after 150 ms the measured voltages seem to decrease almost exponentially like in the previous experiment (Trip of one wind turbine at 10 kV terminal), while the simulated voltages changes to a very slow damped fluctuation. Like in the previous experiment, the measured frequency is probably continuously decreasing because a hydraulic pump is active. But in the simulations, when both the generator and capacitor is disconnected after 150 ms, the transformer and power collection cable are left on an island without rotating machines. The transformer and the cable can be approximated with a resonance circuit with an eigenfrequency of approximately 17 Hz corresponding to 58 ms period time, which corresponds quite well to what can be observed in Figure 85.

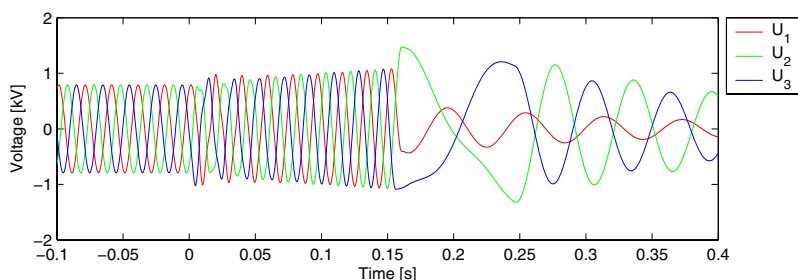


Figure 85: Simulated line to neutral voltages U_{LV} at the 960 V bus of wind turbine #1.

Figure 86 shows the simulated generator currents. Compared to the corresponding measured currents in Figure 40, the overall behaviour is quite similar, with a current drop right after the tripping at $t = 0$ s, followed by an increase in the current until it is disconnected at approximately $t = 150$ ms. However, it looks like the simulated currents increase faster than the measured from $t = 0$ s to $t = 150$ ms.

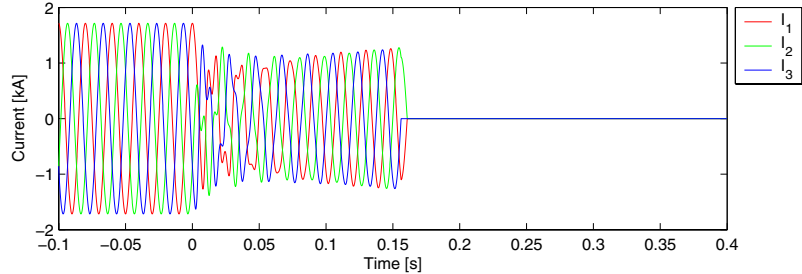


Figure 86: Simulated line currents I_{gen} of the generator of wind turbine #1.

This is confirmed looking at the active and reactive power in Figure 87 and Figure 88. The active power mean value is close to zero after the tripping, while the consumed reactive power increases, which takes place as a combination of increased currents and voltages. Comparisons of fundamental voltages and currents in Figure 89 and Figure 90 confirm this, but the measured currents seem to stabilise after the tripping rather than increase like in the simulation. Again, saturation is a possible explanation for most of the difference, but this has not been validated by simulations including saturation effects.

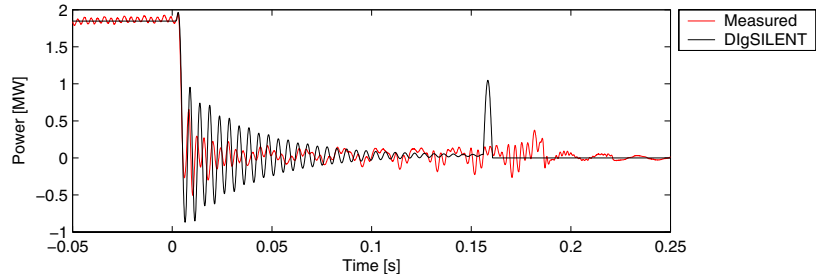


Figure 87: Measured and simulated (DIgSILENT) generator power of wind turbine #1.

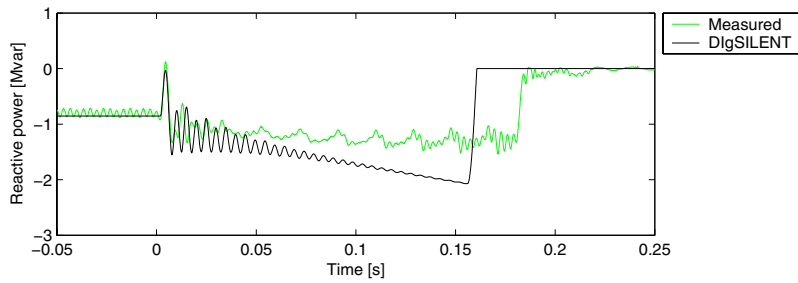


Figure 88: Measured and simulated (DIgSILENT) generator reactive power of wind turbine #1.

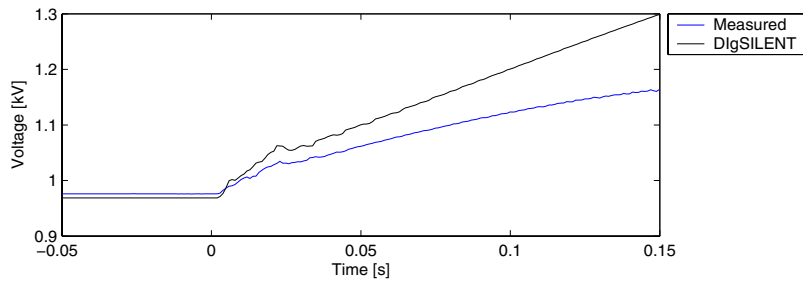


Figure 89: Measured and simulated (DIgSILENT) positive sequence of U_{LV} voltage of wind turbine #1.

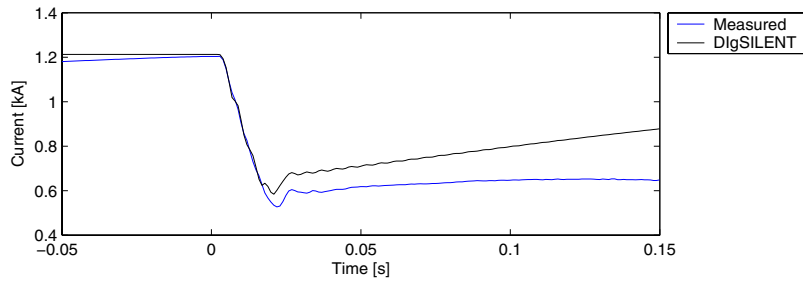


Figure 90: Measured and simulated (DIgSILENT) positive sequence of generator current I_{gen} of wind turbine #1.

Figure 91 and Figure 92 show the measured and simulated mechanical response to the tripping, which is quite similar to the previous experiment.

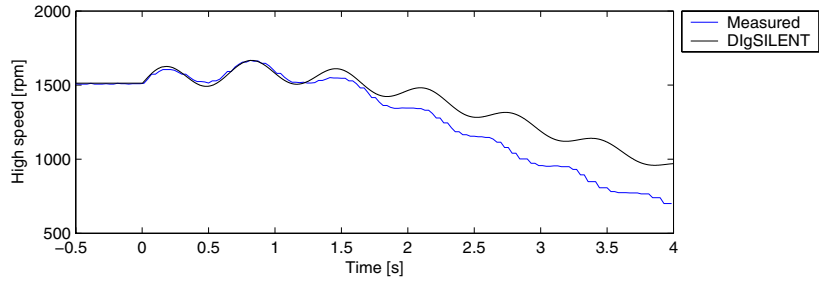


Figure 91: Measured and simulated (DiG SILENT) generator speed of wind turbine #1.

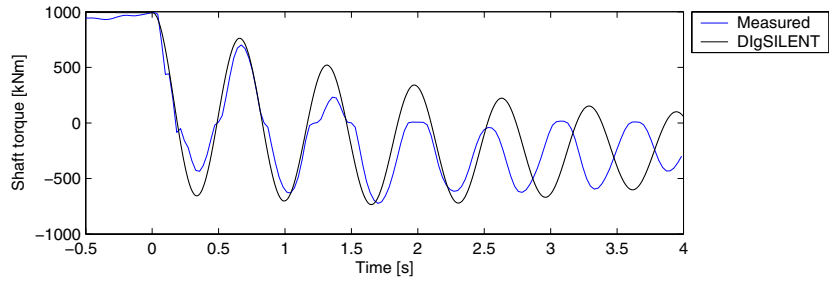


Figure 92: Measured and simulated (DiG SILENT) shaft torque of wind turbine #1.

Figure 93 and Figure 94 show the reactive power on the 10 kV terminals of wind turbine #1 and on the collection cable in Grevinge respectively. It is seen that also this experiment results in a reactive power spike right after the tripping. It is also seen that the size of the spike is larger at the wind turbine terminals than in the substation. This is the case for both simulations and measurements.

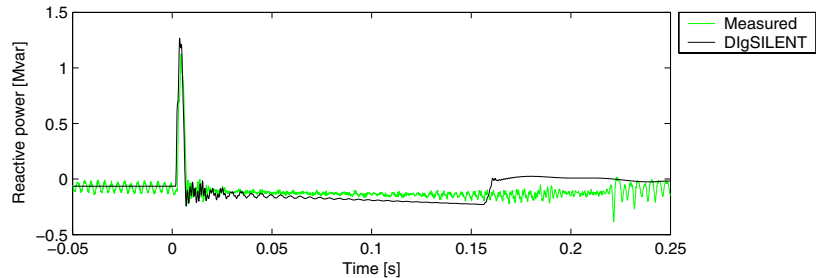


Figure 93: Measured and simulated (DiG SILENT) reactive power at 10 kV terminal of wind turbine #1.

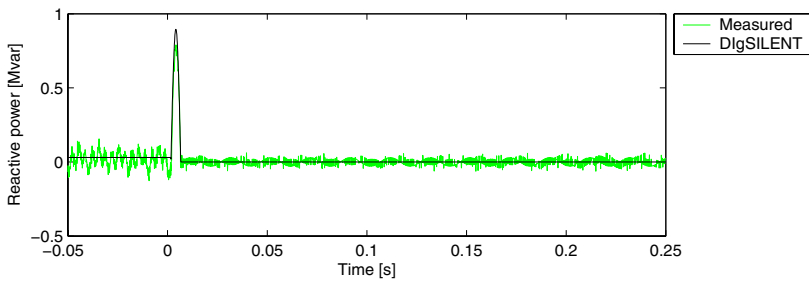


Figure 94: Measured and simulated (DlgsILENT) reactive power at 10 kV collection cable in Grevinge substation.

6.4 Emergency stop

The emergency stop has not been simulated in the present project. The main reason for omitting this simulation is that it will involve the mechanical brake, which is not presently included in the models.

6.5 Islanding of two wind turbines

The experiment “Islanding of two wind turbines” is described in section 5.7. This experiment has been simulated with the EMTDC model. In the present section, we will present the simulation results and compare them to the measurements.

Figure 95 - Figure 98 show the simulated voltages and currents on the 10 kV terminals of wind turbine #2 and wind turbine #6 respectively. Compared to the corresponding measurements in Figure 59 - Figure 60 and Figure 62 - Figure 63, the simulated voltages show higher transients right after the tripping than what is observed in the measurements. Moreover, the simulated voltages differ after the generators are tripped like in the previous experiments. The simulated currents look more like the measured.

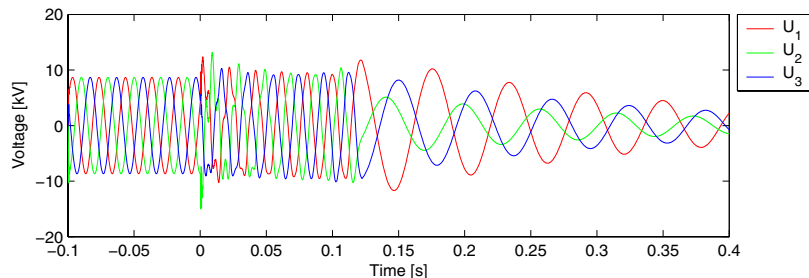


Figure 95: Simulated (EMTDC) voltages at 10 kV terminal of wind turbine #2.

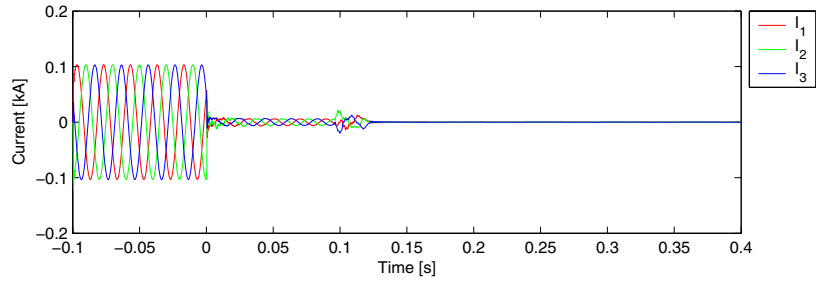


Figure 96: Simulated (EMTDC) currents at 10 kV terminal of wind turbine #2.

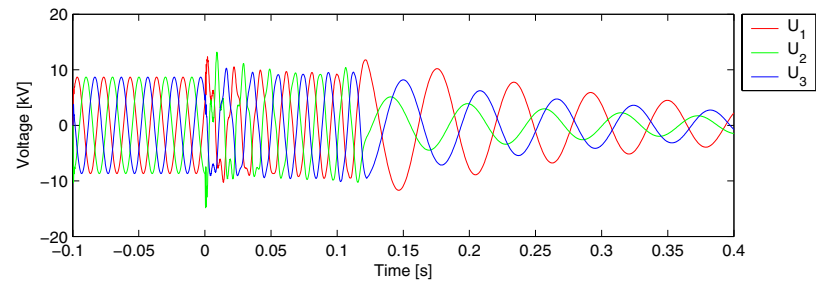


Figure 97: Simulated (EMTDC) voltages at 10 kV terminal of wind turbine #6.

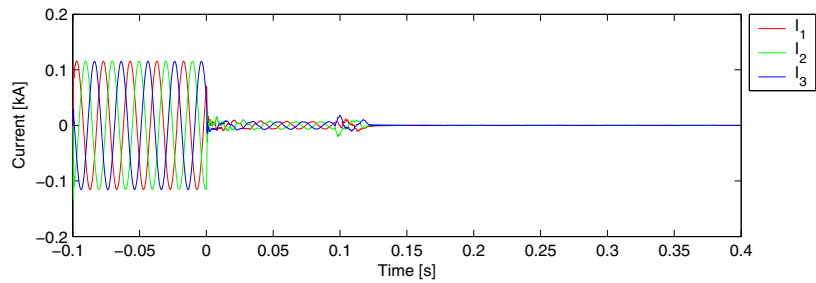


Figure 98: Simulated (EMTDC) currents at 10 kV terminal of wind turbine #6.

Figure 99 and Figure 100 compares the measured active and reactive power. It is seen that the reactive power spike is not present in these simulations, which is because the breakers have been assumed to disconnect completely immediately after they are activated. This assumption was made in the EMTDC simulations because vacuum breakers are used, but apparently an arc is still present until the first zero crossing of the current. The immediate disconnection in the simulation is probably also the reason for the transients in the simulated voltages in Figure 95 and Figure 97.

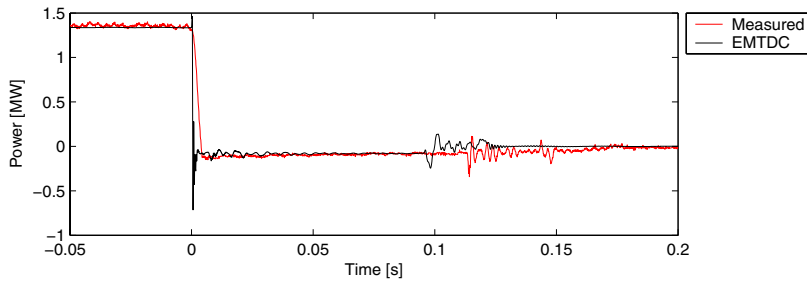


Figure 99: Simulated (EMTDC) and measured power at 10 kV terminal of wind turbine #2.

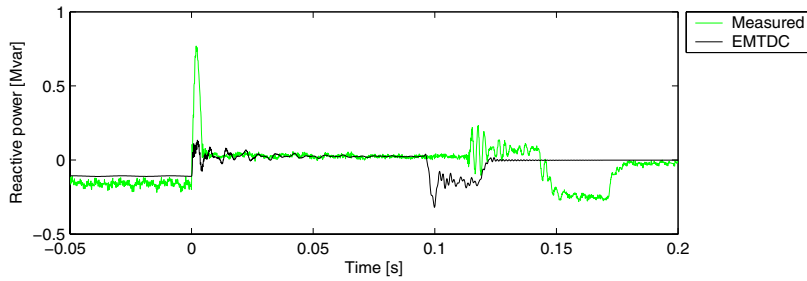


Figure 100: Simulated (EMTDC) and measured reactive power at 10 kV terminal of wind turbine #2.

The positive sequence of the measured and simulated voltage are compared in Figure 101. Like in the previous experiments (simulated with DIgSILENT), it is seen that the simulated voltages in the island increase significantly faster than the measured. Also in this case, saturation is a possible explanation.

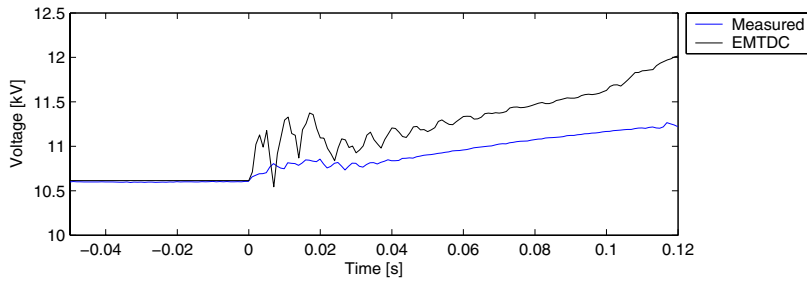


Figure 101: Simulated (EMTDC) and measured voltage (positive sequence) at 10 kV terminal of wind turbine #2.

6.6 Voltage change due to tripping

The experiment “Voltage change due to tripping” is described in section 5.8. This experiment has been simulated with the EMTDC model and the DIgSILENT model. In the present section, we will present the simulation results and compare them to the measurements.

Figure 102 shows the simulated voltages U_{LV} of the present experiment. The voltage change is so small that it cannot be seen on the instantaneous values, which is similar to the measurement result in Figure 66.

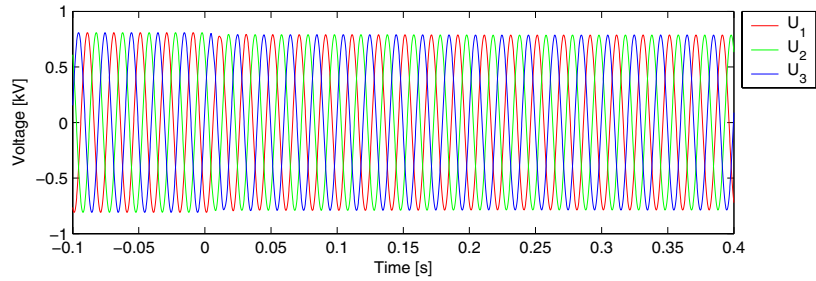


Figure 102: Simulated (EMTDC) voltages U_{LV} at the low voltage terminal of wind turbine #1.

However, looking at the RMS value of the fundamental component in Figure 103, the voltage changes are clearly observed. It is seen that the measured voltage change is smaller than the simulated. The reason for the difference could well be that the active and reactive power produced by wind turbine #2 is not known, and was simply assumed to be the average of wind turbine #1 and #6.

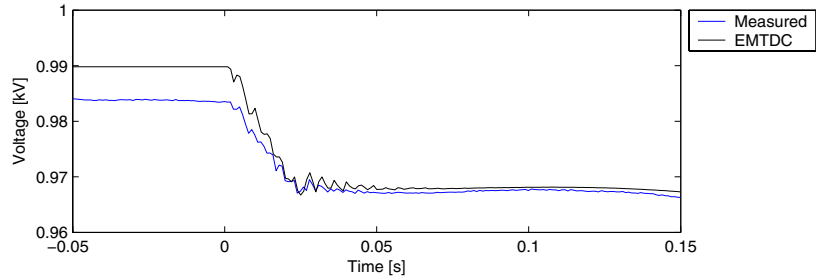


Figure 103: Fundamental component of the measured and simulated (EMTDC) voltages U_{LV} at the low voltage terminal of wind turbine #1.

The frequencies of the fundamental are compared in Figure 104. It is seen that the phase step due to the tripping causes the frequencies to dip.

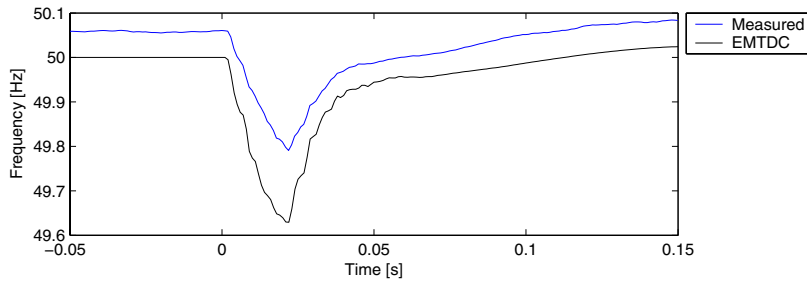


Figure 104: Fundamental frequency of the measured and simulated (EMTDC) voltages U_{LV} at the low voltage terminal of wind turbine #1.

The simulated generator currents are shown in Figure 105. An immediate comparison to the measured currents in Figure 67 indicates that the simulated currents show similar current spikes as the measured in the first line period after the tripping.

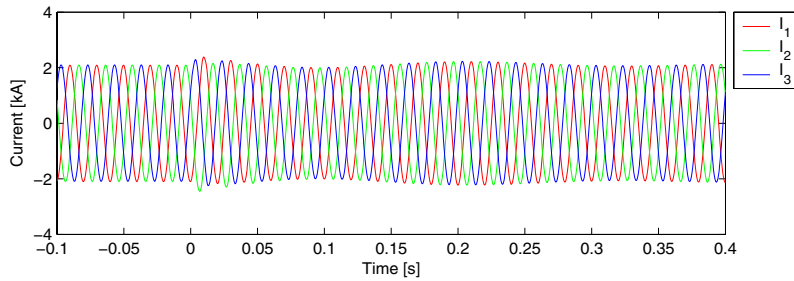


Figure 105: Simulated (EMTDC) generator currents I_{gen} of wind turbine #1.

Looking at the positive sequence of the fundamental component of the generator currents in Figure 106, this is confirmed. The measured current is on the way up before the voltage distortion (at $t = 0$ s) because of turbulence, and this change continues after the voltage distortion. The turbulence is not included in the present simulations.

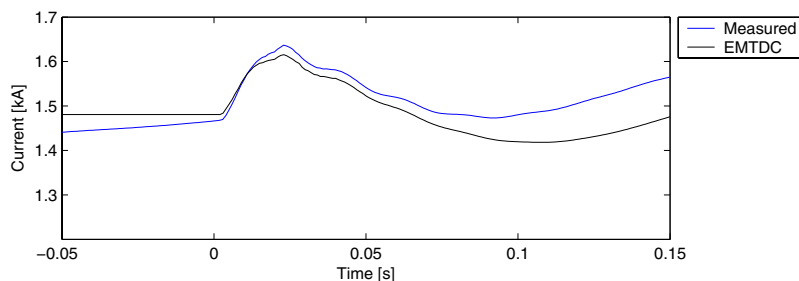


Figure 106: Positive sequence of measured and simulated (DIgSILENT) generator currents I_{gen} of wind turbine #1.

Figure 107 and Figure 108 compares measured and simulated active and reactive power of the generator. It is seen that the simulation has been fitted to have the same power as measured at $t = 0$, but this selection implies a simulated reactive power consumption, which is approximately 100 kvar higher than the measured reactive power. This is because of the necessary approximations in the generator modelling as discussed in section 3.3.1.

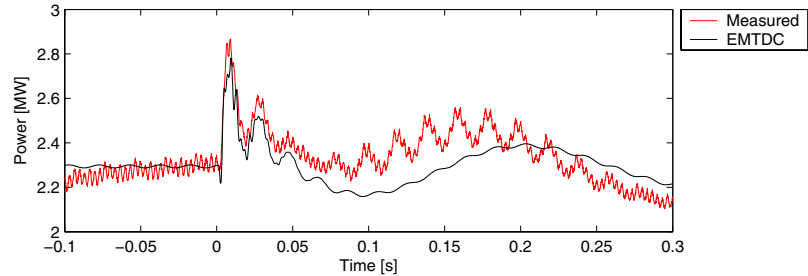


Figure 107: Measured and simulated (EMTDC) generator power P_{gen} of wind turbine #1.

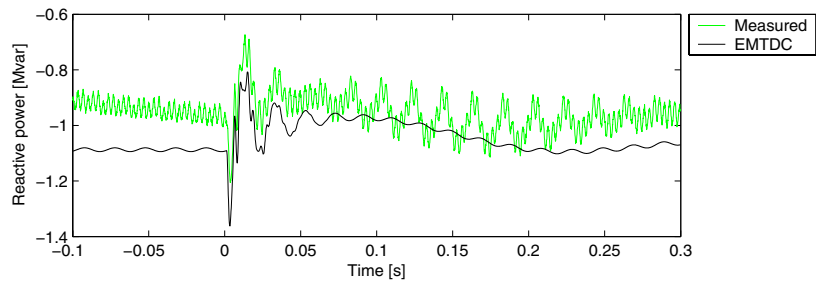


Figure 108: Measured and simulated (EMTDC) generator reactive power Q_{gen} of wind turbine #1.

Figure 109 and Figure 110 show active and reactive power of the similar simulation in DIgSILENT. Compared to Figure 107 and Figure 108, it is seen that the simulations are quite similar, only the fundamental component in EMTDC steady state are not present in DIgSILENT, and also not in the measurements before the tripping.

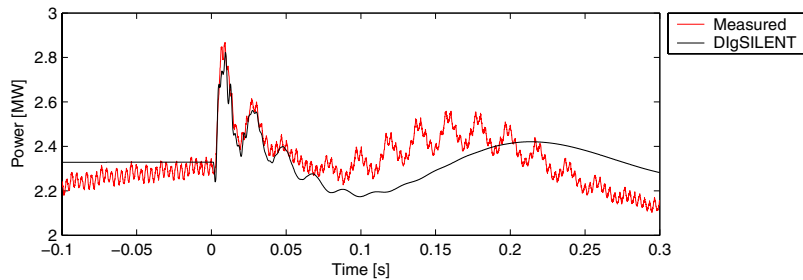


Figure 109: Measured and simulated (DiGSILENT) generator power P_{gen} of wind turbine #1.

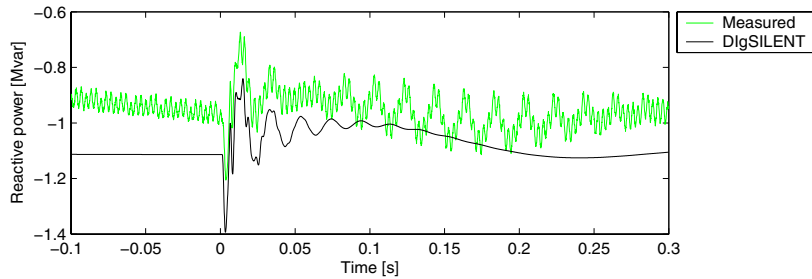


Figure 110: Measured and simulated (DiGSILENT) generator reactive power Q_{gen} of wind turbine #1.

Figure 111 compares measured and simulated shaft torque for $t = -1$ s to $t = 3$ s. Obviously, there is a distinct difference, which is due to the omission of turbulence in the simulations as described above. Apparently, the special distribution of the turbulence in the rotor plane during the 4 seconds where the experiment took place was fairly extreme, causing the turbulence generated 3 p component (around 0.9 Hz) of the torque to be very high (the measured oscillation is 0.8-0.9 Hz, slightly different because the turbulence changes causing also the frequency to vary slightly). It would be possible to simulate a turbulence gust, which would result in the measured shaft torque, but this has not been implemented. Anyway, the conclusion that the turbulence has much larger influence on the shaft torque than the voltage change resulting from the present experiment is evident.

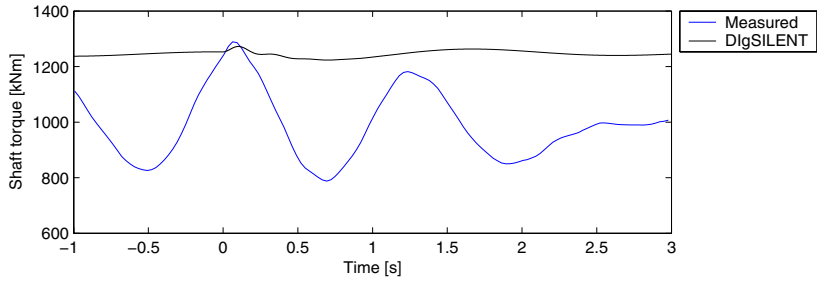


Figure 111: Measured and simulated (DiGILENT) shaft torque of wind turbine #1.

This is also the case with the generator speed compared in Figure 112. The simulation shows a distinct oscillation with the generator frequency at approximately 5 Hz. But the resolution of the speed measurement is too rough to reveal the possible agreements with the simulations, and the correlation between speed in Figure 112 and torque in Figure 111 is dominating the visible speed variations.

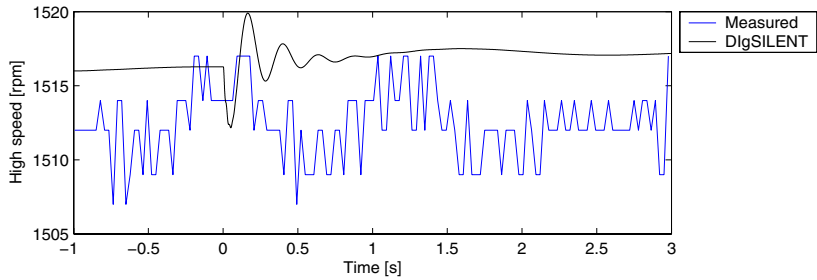


Figure 112: Measured and simulated (DiGILENT) generator speed of wind turbine #1.

6.7 Voltage change due to tap position changing

The experiment “Voltage change due to tap position changing” is described in section 5.9. This experiment has been simulated with the DiGILENT model. In the present section, we will present the simulation results and compare them to the measurements.

Figure 113 shows the measured voltages, whereas Figure 114 compares the RMS value of the positive sequence of the fundamental to the measurements. Different from the previous test, both measured and simulated voltages have a significant dynamic contribution with a time constant around 250 ms. It is also seen that the simulation does not have the distinct increment which was observed in a number of repeated experiments as mentioned in section 5.9.

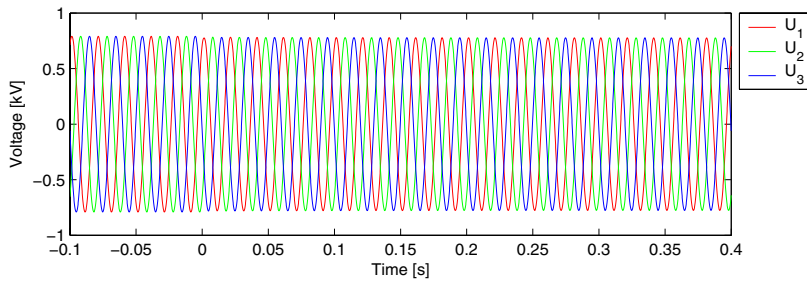


Figure 113: Simulated (DIgSILENT) voltages U_{LV} at the low voltage terminal of wind turbine #1.

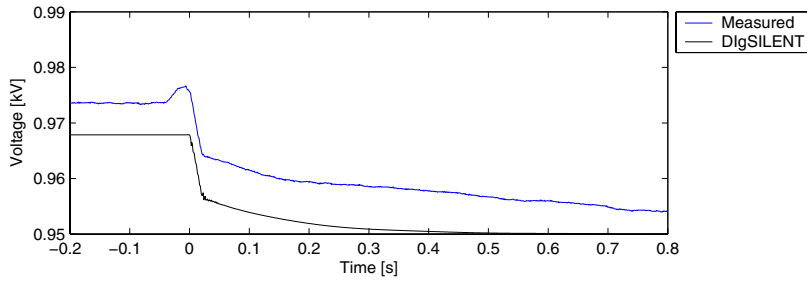


Figure 114: Fundamental component of the measured and simulated (DIgSILENT) voltages U_{LV} at the low voltage terminal of wind turbine #1.

The simulated currents and the corresponding positive sequence are shown in Figure 115 and Figure 116 respectively. Figure 116 shows some agreement between the dynamics of the measurements and simulations in the first 50 ms after the tap change, but apart from that the current is strongly influenced by turbulence as in the previous case. However, it is difficult to assess the agreement between the simulation and the measurement of the tap changing, because the tap change has a relatively small influence on the dynamics, compared to the influence of turbulence.

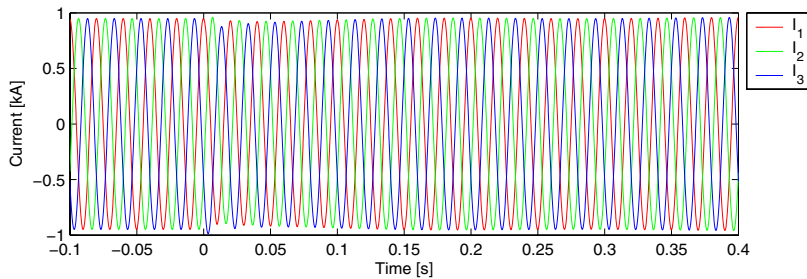


Figure 115: Simulated (DIgSILENT) generator currents I_{gen} of wind turbine #1.

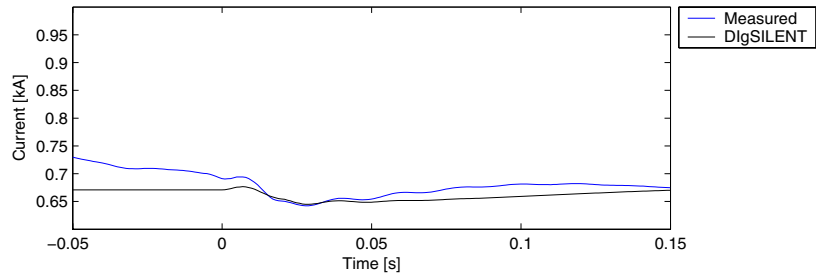


Figure 116: Positive sequence of measured and simulated (DIgSILENT) generator currents I_{gen} of wind turbine #1.

7 Conclusions

The main conclusions of the present work are listed below:

- Comparisons between simulations of a symmetric short circuit with EMTDC and the EMT models in DIgSILENT show an extremely close agreement between simulations with the same basic options, i.e. same generator steady state model, no saturation and same time steps. A similar simulation case has been selected for a Benchmark model, because the comparison has given high trust in the simulation results.
- Comparisons between simulations with DIgSILENTs EMT model and RMS model show that if no fast relays are tripped, the long-term stability of the system is not affected by the generator stator flux transients in the EMT model, and consequently the dynamic system stability can be studied using the RMS simulations, which is also traditionally done in stability simulation tools like PSS/E.
- Comparisons of EMTDC simulations with and without saturation reveal up to 10 % difference in the simulated peak currents with and without saturation, but the difference is only distinct in the first line period after establishing the short circuit and after clearing the short circuit.
- Saturation may well be important in the tripping cases, as many of the observed differences between measurements and simulations could be due to lack of saturation in the simulations. Especially, it has generally been observed that the simulated voltages in the tripped (one or two wind turbine) islands increase much faster than the measured voltages. However, this statement has not been confirmed by simulations including saturation effects.
- Saturation of all reactance in a generator and saturation of the magnetising reactance in a transformer can be modelled in EMTDC. In DIgSILENT, modelling of saturation in a generator is not possible, but the magnetising reactance of the transformer can be modelled with saturation. The inclusion of saturation in the magnetising reactances will limit the voltage, and therefore it may be possible with the available DIgSILENT options to improve the simulation of the volt-

age increase in the islanding cases. But it will probably not be possible with the present DIgSILENT options to improve the simulation in the short circuit cases, because the higher short circuit currents are due to saturation in the serial reactances in the generator. The EMTDC options for saturation should be sufficient to improve simulations in both cases.

- Dynamic inflow should be included in future aerodynamic models for transient simulations, as this is a possible explanation of observed differences between measurements and simulations.
- Backlash in the gearboxes should also be included in future models, comparisons to measurements show that backlash has a distinct influence on the shaft torque during zero crossings, and the comparisons also indicates that backlash effects the oscillation frequency on the shaft
- The EMTDC simulations show a much more instantaneous drop than the DIgSILENT simulations of current, active and reactive power when a breaker is activated. The explanation is simple and gives a very good idea of how difficult it is to make two teams with different tools create identical transient simulations. The teams had overlooked to agree on the expected way the different breakers should work. The EMTDC team with its utility background opted for instantaneous breaking for the 10 kV breakers and breaking at current zero for the 0,96 kV breakers. The DIgSilent team opted for breaking at current zero for all breakers. The measurements proved the DIgSilent team right.
- Data for the protection system has been invested very carefully in the project, but still the comparisons between measurements and simulations show that it has been quite difficult to get a precise idea of how and when the breakers cutting out the capacitors of the turbine operates. NEGMicon provided all the data one could ask for and more regarding relay types, settings, drop out voltages - of all the different components somehow included in the switching event. So the teams agreed on each drawing their own conclusions on NEGMicons data – each choosing a proper control, protection and timelag setup – each doing their best to forecast the upcoming measurements.
- Comparisons of measurements and simulations in island operation show very poor agreement after both generators and capacitors are disconnected. The reason for the difference is probably that a hydraulic pump is still on the island grid. However, this does not mean that it is essential to include the hydraulic pump in the modelling, because it is expected to have only little influence on the ride through capability of the wind turbine in case of a grid fault. However, this example shows that a wind turbine is a very complex unit, which makes modelling a challenging task.

References

- [1] Energy 21. The Danish Government's Action Plan. The Danish Energy Agency, April 1996.

- [2] Tilslutningsbetingelser for vindmølleparker tilsluttet eltransmissionsnettet. 1. udgave. Elkrafts Netudvalg Juli 1999.
- [3] Specifications for connecting wind farms to the transmission network. Second edition. Eltra transmission system planning April 2000.
- [4] IEC 61400-21. Ed.1: Wind turbine generator systems – Part 21: Measurement and assessment of power quality characteristics of grid connected wind turbines. Final Draft International Standard 88/144/FDIS International Electrotechnical Commission, IEC 2001-07-01.
- [5] A.I.Estanqueiro, R.F.Aguiar, J.A.G.Saraiva, R.M.G.Castro and J.M.F.D.Jesus. On the effect of utility grid characteristics on wind park power output fluctuations. Proceedings of British Wind Energy Conference BWEA'15. York 1993.
- [6] P. Sørensen, A.D. Hansen, L. Janosi, J. Bech, B. Bak-Jensen. Simulation of interaction between wind farm and power system. Risø-R-1281(EN) (2001)
- [7] V.Akhmatov, H.Knudsen, A.H.Nielsen. Advanced simulation of windmills in the electric power system. Electrical Power and Energy Systems 22, p.421-434. Elsevier 2000.
- [8] P. Christensen, Integration of large scale off-shore wind power plants - System aspects, STATCOM stabilization and VSC HVDC connection. *Proc 1st International workshop on feasibility of HVDC transmission networks of offshore wind farms*. Stockholm, SE, 2000.
- [9] DIgSILENT note on asynchronous machine models.
- [10] F. Iov. Analysis of full and reduced order models for squirrel cage and wound rotor induction machine. Internal note. Aalborg, DK, 2001.
- [11] T.J. Larsen, M.H. Hansen, & F. Iov, *Generator dynamics in aeroelastic analysis and simulations*. (Risø-R-1395(EN) , DK, 2003)
- [12] S.Øye, Dynamic stall - simulated as time lag of separation. 1991. Proceedings of the 4th IEA Symposium on the Aerodynamics of Wind Turbines, McAnulty, K.F. (Ed), Rome, Italy.
- [13] H. Bindner. Active control: Wind turbine model. Risø-R-920(EN) (1999) 37 p
- [14] P. Kundur, *Power system stability and control*, EPRI, McGraw-Hill, 1994.
- [15] V. Akhmatov, Modelling of variable speed wind turbines with double-fed induction generators in short-term stability investigations. *Proc 3rd International workshop on feasibility of HVDC transmission networks of offshore wind farms*. Stockholm, SE, 2002.

Appendix A Benchmark model

A.1 General

The present Benchmark model provides the description of a simplified simulation case of a short circuit in a reduced wind power installation. The selected case is illustrated in the single line diagram in Figure A-1.

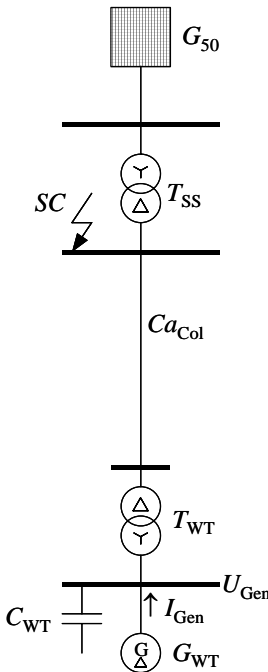


Figure A-1 Single line diagram of Benchmark case

A.2 50 kV grid

The 50 kV grid G_{50} in Figure A-1 is modeled by a Thevenin equivalent with the data given in Table 1. The phase of the voltage is a 0 deg (i.e. first line to neutral is a sinus).

U_{Th}	50 kV
R_{Th}	2.1156 Ω
X_{Th}	8.2998 Ω

Table 1. 50kV grid (G_{50}) data

A.3 50/10 kV transformer

The 50/10.5 kV transformer T_{ss} in Figure A-1 is modeled by a T-equivalent with the data given in Table 2. All reactances are without saturation. No-load losses are not included. The phase connection is YNd5. The transformer is directly grounded.

S_n	16 MVA
U_p	50 kV
U_s	10.5 kV
R_p	0.4052 Ω
X_p	7.655 Ω
X_m	19530 Ω
R'_s	0.4052 Ω
X'_s	7.655 Ω

Table 2. 50/10 kV transformer (T_{Gr}) data

A.4 Short circuit

SC in Figure A-1 is a 3 phase short circuit, duration 100 ms, error impedance before the short circuit is 1 $M\Omega$ (star impedance). The short circuit impedance is 0.00011 Ω (star impedance, corresponds to 0.00033 Ω delta impedance in EMTDC).

A.5 10 kV collection cable

The wind farm 10 kV collection cable Ca_{Col} in Figure A-1 is modeled by a π -equivalent with the data given in Table 3.

C_1	1.58 μF
R	0.7568 Ω
X	0.4473 Ω
C_2	1.58 μF

Table 3. Wind farm 10 kV collection cable (Ca_{Col}) data

A.6 10/0.96 kV transformer

The 10/0.96 kV transformer T_{WT1} in Figure A-1 is modeled by a T-equivalent with the data given in Table 4. All reactances are without saturation. No-load losses are not included. The phase connection is Dyn5. The transformer is directly grounded.

S_n	2 MVA
U_p	10.5 kV
U_s	0.96 kV
R_p	0.2756 Ω
X_p	1.654 Ω
X_m	6890 Ω
R_s'	0.2756 Ω
X_s'	1.654 Ω

Table 4. 10/0.96 kV transformer (T_{WT1}) data

A.7 Wind turbine capacitor bank

The 0.96 kV capacitor bank in the wind turbine C_{WT} in Figure A-1 is delta connected, with the capacity $C_A = 1333 \mu\text{F}$ in series with $R_A = 0.003 \Omega$.

A.8 Wind turbine generator

The induction generator in the wind turbine G_{WT} in Figure A-1 is modeled by a T-equivalent with the data given in Table 5.

S_n	2.3 MVA
U_n	0.96 kV
N_0	1500 rpm
R_s	0.004 Ω
X_s	0.05 Ω
X_m	1.6 Ω
R_r'	0.004 Ω
X_r'	0.05 Ω

Table 5. Induction generator data

A.9 Mechanical system

The mechanical system is modelled according to Figure A-2

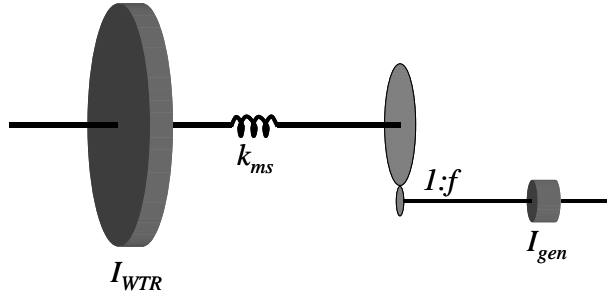


Figure A-2. Mechanical system

The data for the model is given in Table 6.

I_{WTR}	$4.176 \cdot 10^6 \text{ kg m}^2$
I_{gen}	93.22 kg m^2
k_{ms}	$8.949 \cdot 10^7 \text{ Nm / rad}$
f	80

Table 6. Mechanical system data

A.10 Simulation options

The aerodynamic torque is adjusted to give 2MW electrical power from the wind turbine generator G_{WT} and kept constant through and after the short circuit.

The simulation are performed with fixed time steps $T_{sim} = 10 \mu\text{s}$. The simulated time series are saved with time steps $T_{sim} 100 \mu\text{s}$, i.e. data is reduced with a factor 10 before it is saved.

A.11 Simulation results

The simulation results for EMTDC as well as DIgSILENT simulations are shown below, to give an indication of the acceptable agreement.

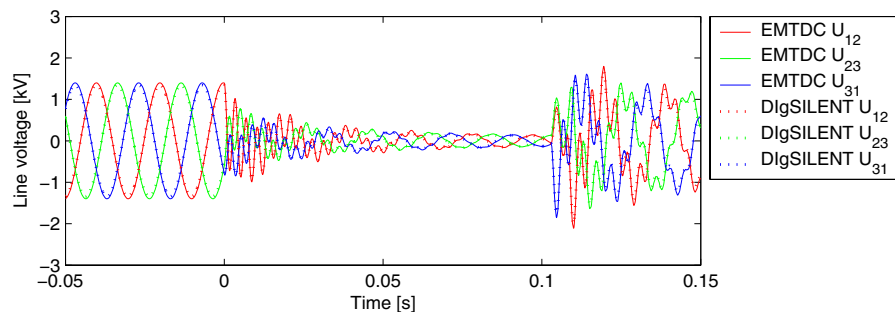


Figure A-3 Generator voltages U_{gen} during and around the short circuit period.

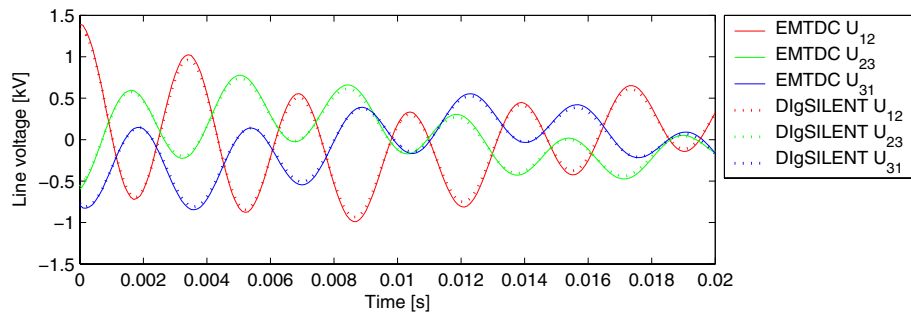


Figure A-4 Generator voltages U_{gen} during the first 20 ms (1 line period) of the short circuit.

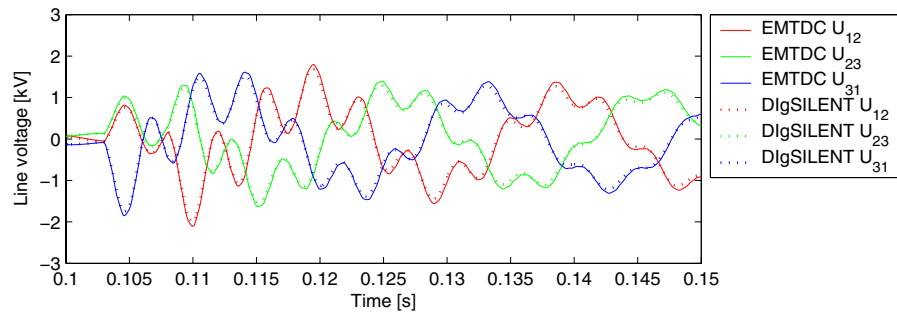


Figure A-5 Generator voltages U_{gen} in the first 50 ms (2.5 line periods) right after clearance of the short circuit

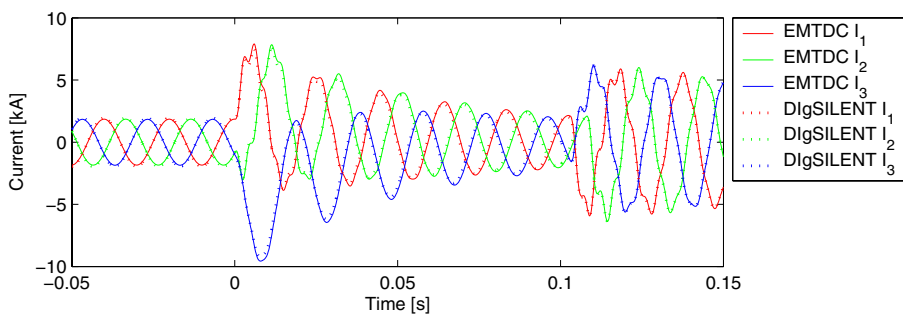


Figure A-6 Generator currents I_{gen} during and around the short circuit

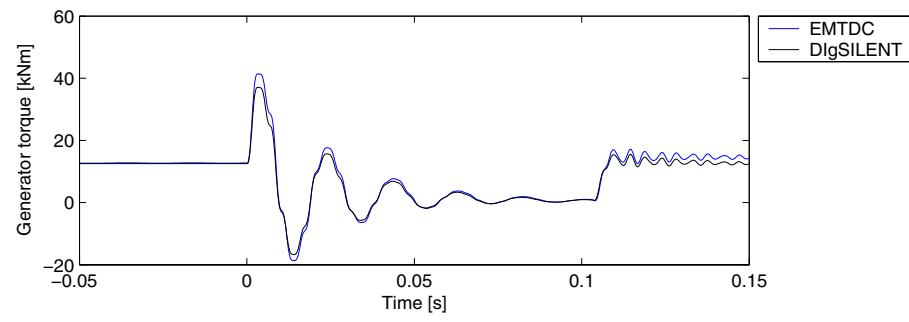


Figure A-7 Generator torque T_{gen} during and around the short circuit

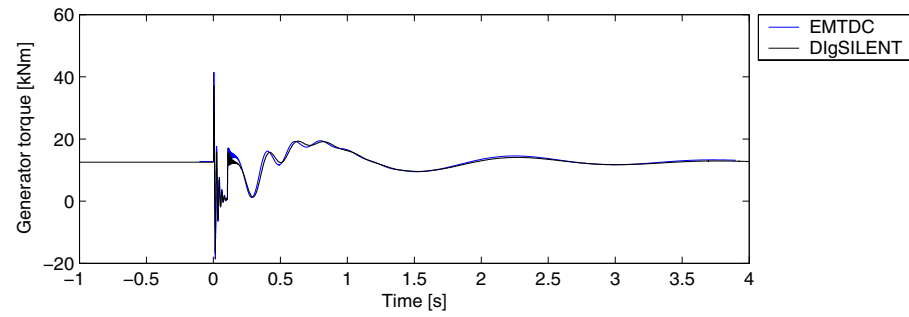


Figure A-8 Longer-term generator torque T_{gen} during and around the short circuit

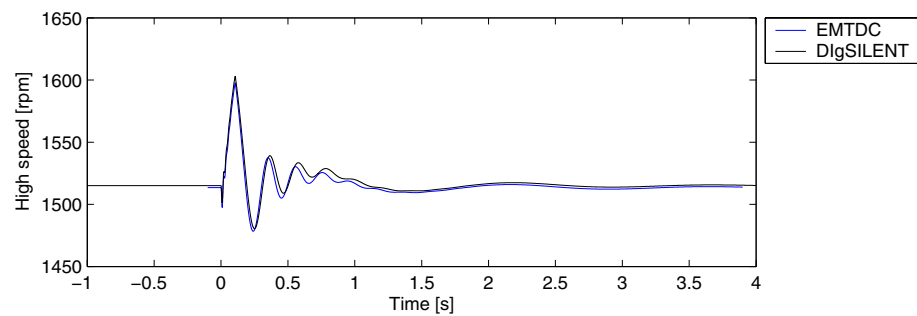


Figure A-9 Longer-term generator speed fluctuations caused by the short circuit

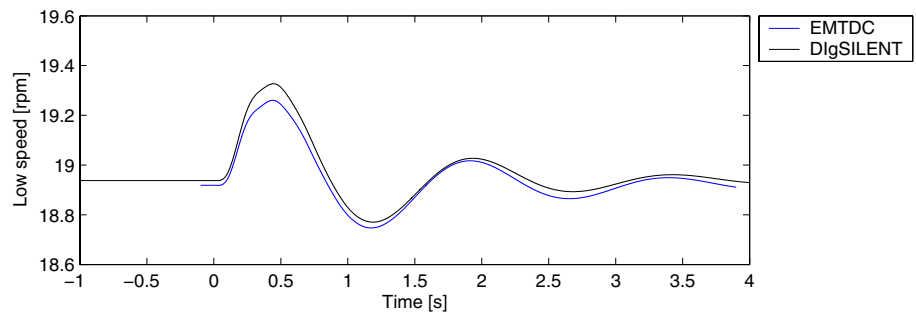


Figure A-10 Longer-term wind turbine rotor (WTR) speed fluctuations caused by the short circuit

Bibliographic Data Sheet**Risø-R-1331(EN)**

Title and authors

Simulation and verification of transient events in large wind power installations

Poul Sørensen, Anca D. Hansen, Peter Christensen, Morten Mieritz, John Bech,
Birgitte Bak-Jensen and Hans Nielsen

ISBN	ISSN		
87-550-3030-0; 87-550-3031-9 (Internet)	0106-2840		
Department or group	Date		
Wind Energy Department	October 2003		
Groups own reg. number(s)	Project/contract No(s)		
1115024-1	Bro-91.054 (FU 1103)		
Pages	Tables	Illustrations	References
80	6	124	15

Abstract (max. 2000 characters)

Models for wind power installations excited by transient events have been developed and verified. A number of cases have been investigated, including comparisons of simulations of a three-phase short circuit, validation with measurements of tripping of single wind turbine, islanding of a group of two wind turbines, and voltage steps caused by tripping of wind turbines and by manual transformer tap-changing. A Benchmark model is also presented, enabling the reader to test own simulation results against results obtained with models developed in EMTDC and DIgSILENT.

Descriptors INIS/EDB

COMPUTERIZED SIMULATION; ELECTRICAL TRANSIENTS;
MATHEMATICAL MODELS; VERIFICATION; WIND POWER PLANTS